Check for updates

Robust direct digital-to-biological data storage in living cells

Sung Sun Yim [1], Ross M. McBee [1,2], Alan M. Song[1], Yiming Huang [1,3], Ravi U. Sheth[1,3] and Harris H. Wang [1,4] ✉

DNA has been the predominant information storage medium for biology and holds great promise as a next-generation high-density data medium in the digital era. Currently, the vast majority of DNA-based data storage approaches rely on in vitro DNA synthesis. As such, there are limited methods to encode digital data into the chromosomes of living cells in a single step. Here, we describe a new electrogenetic framework for direct storage of digital data in living cells. Using an engineered redox-responsive CRISPR adaptation system, we encoded binary data in 3-bit units into CRISPR arrays of bacterial cells by electrical stimulation. We demonstrate multiplex data encoding into barcoded cell populations to yield meaningful information storage and capacity up to 72 bits, which can be maintained over many generations in natural open environments. This work establishes a direct digital-to-biological data storage framework and advances our capacity for information exchange between silicon- and carbon-based entities.

D NA is a ubiquitous molecule in biology that stores life's heritable information. In the digital era, DNA is also poised to become a next-generation universal data medium[1] because of its high-density storage capacity (petabytes per gram)[2], long-term stability (even in harsh environments; half-life of >500 years)[3] and low risk of technical obsolescence due to the expanding interest in DNA[4]. Data storage in DNA has progressed technologically over the past decade[4], as strategies to physically isolate and selectively access portions of the stored data[5,6] as well as algorithmic advances to optimize data encoding and retrieval[2,7] have greatly improved the scalability and practicality of DNA information storage. However, current DNA-based data-storage methods still rely mainly on in vitro iterative chemical or enzymatic synthesis of DNA strands[4,8].

At the same time, recent advances in CRISPR (clustered regularly interspaced short palindromic repeats) and recombinase technologies have led to the development of numerous DNA-based cellular recording systems to interrogate various biological processes[9,10], such as lineage tracing for organismal development[11–13] and real-time recording of horizontal gene transfer events[14]. These cellular data recorders offer the capacity to measure biologically relevant signals[15–19] in places that are otherwise difficult to access, such as inside the body[20,21], and over time[22]. Furthermore, the stored data in DNA can be coupled to gene regulation to directly report cellular states[23] or control cellular logic operations[24]. These excellent features and the inherent compatibility of DNA-based data storage with biological systems have suggested the potential use of living cells as a physical medium for data in DNA to provide more protection (for example, in radiation- and heat-resistant spores) and enable facile data duplication and amplification (via cell growth and replication)[4,10]. However, such in vivo data storage approaches largely build on in vitro synthesized DNA strands[25,26] due to the limited capacity to manipulate DNA sequences directly in vivo[4]. This challenge motivates the exploration of easy and scalable transmission of digital data into biological systems (direct encoding) and back (decoding by sequencing).

Direct information exchange between electronics and biology has tremendous potential to transform our ability to analyze, store and communicate information[27–29]. The classic example is the direct electrical simulation or recording of neurons via ionic potentials and currents[27]. Beyond ionic potentials, the reduction–oxidation (redox) state of a cell, which is involved in a wide range of biological processes, is also amenable to physiological measurement and perturbation with electronic devices. Recently, redox-responsive biomolecules such as phenazines have been used in several electrochemical strategies to interrogate a range of biological activities[30,31] and to control gene expression in living cells[32,33], where the redox status of the biomolecules could be measured or manipulated by application of electronic potentials. In theory, these approaches could also be used for direct electrochemical encoding of data into DNA in living cells. In practice, however, the utility of such in vivo DNA recording systems depends heavily on the efficiency, robustness and scalability of the underlying electrogenetic circuits, which may require extensive engineering and optimization.

Here, we describe a scalable and direct strategy—'data recording in vivo by electrical stimulation' (DRIVES)—to encode digital data into the genomes of living cells without the need to synthesize DNA in vitro (Fig. 1a). By using electrical signals to tune redox biomolecules and sensors in cells, our framework enables the direct transfer of digital data from a computer to living cells. With a CRISPR-based DNA recorder, we applied this approach to write all possible states of a 3-bit binary data stream into living cells, which can be multiplexed to store larger amounts of information by barcoding cell populations. Data stored in these 'living hard drives' are stably maintained and effectively protected—over multiple cell generations—from external environments where naked DNA would otherwise be degraded. This study provides a foundation to further advance in vivo DNA data storage and direct communication with living cells.

Results

Development of a cellular electrogenetic DNA writer. Previously, we have described a directional DNA writing system using CRISPR

[1]Department of Systems Biology, Columbia University, New York, NY, USA. [2]Department of Biological Sciences, Columbia University, New York, NY, USA. [3]Integrated Program in Cellular, Molecular, and Biomedical Studies, Columbia University, New York, NY, USA. [4]Department of Pathology and Cell Biology, Columbia University, New York, NY, USA. ✉e-mail: hw2429@columbia.edu
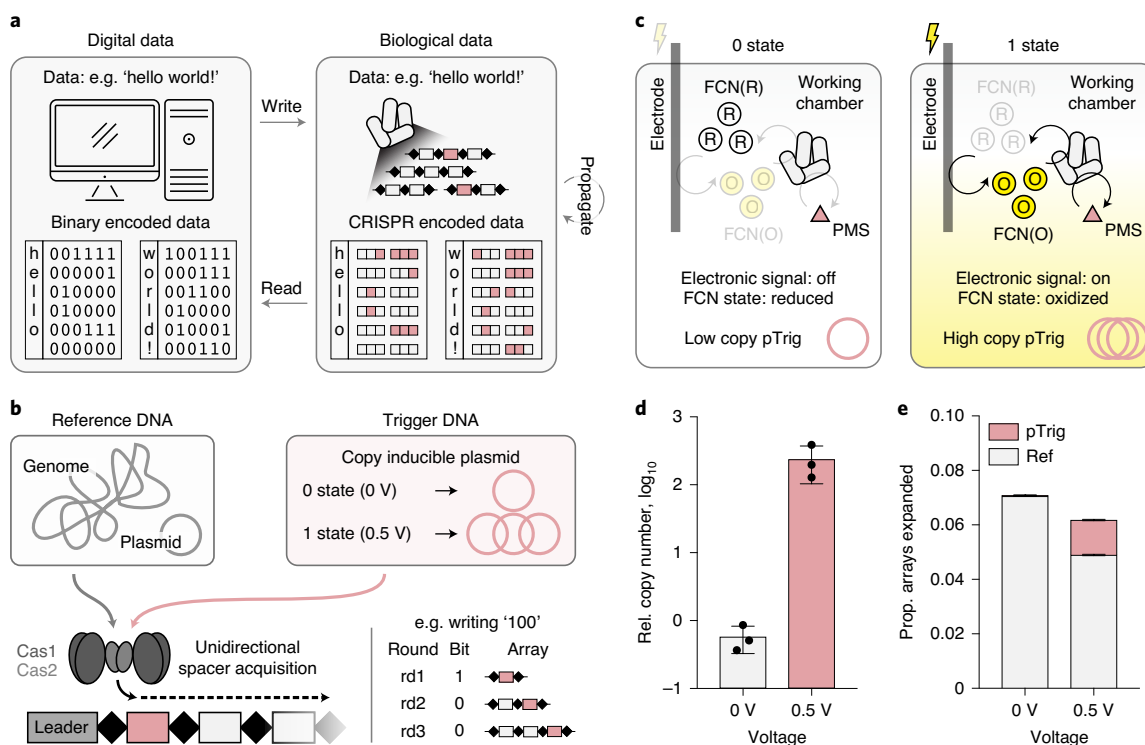
Fig. 1 | Direct digital-to-biological data storage into CRISPR arrays. a, Digital information can be directly encoded into CRISPR arrays of a bacterial population using electronic signals. The cell population can then be archived for long-term storage, propagated for data amplification and sequenced for data retrieval. **b**, Overexpression of the Cas1–Cas2 complex results in constant incorporation of new spacers into CRISPR arrays of a cell population. Electronic signals induce a change in abundance of a copy-number-inducible plasmid (pTrig) and thus the proportion of pTrig-derived spacers. **c**, At the 0 state, the electrical signal is not applied (0.0 V) to keep FCN(R) and PMS reduced and the pTrig copy number is low. At the 1 state, the electrical signal (0.5 V) oxidizes FCN(R) and PMS, activating the *soxS* promoter to increase the pTrig copy number. FCN(R), ferrocyanide; FCN(O), ferricyanide; PMS, phenazine methosulfate. **d,e**, The relative copy number of pTrig (**d**) and the proportion of expanded CRISPR arrays and source of the new spacers (**e**) without (0 V) and with (0.5 V) electrical signal for 14 h. Ref, genome- and pRec-derived spacers; pTrig, pTrig-derived spacers. All measurements are based on three biological replicates. Error bars represent the s.d. of three biological replicates.

spacer acquisition to record user-defined signals in bacteria (Fig. 1b)[22]. We sought to build on this system for its directional feature in writing information and its capabilities of temporal recording and multiplexing for scaling. To directly couple an electrical signal for biological recognition, we explored the use of redox molecules and a redox-responsive SoxRS regulon[33] to convert the cell's electrochemical state into a change in gene expression (Extended Data Fig. 1a), thus coupling the copy number of the plasmid to oxidative stress. Oxidative stress in the cells could then be induced with phenazine methosulfate (PMS) in a dose-dependent manner (Extended Data Fig. 1b). We further tested ferri/ferrocyanide (oxidized, FCN(O); reduced, FCN(R)) as an alternate electron acceptor and used anaerobic growth conditions to exclude the interference of oxygen to improve control of the redox conditions (Extended Data Fig. 1c)[33].

To parallelize electrochemical modulation across multiple cell populations, we constructed a 24-chamber electrochemical redox controller that independently delivers a digital electrical pulse (off, 0 V; on, +0.5 V) to each chamber (Methods and Extended Data Fig. 2). After optimization of the experimental conditions, including inducer concentrations and induction time (Extended Data Fig. 1d–g), we could robustly modulate cell populations using an electrical signal to induce a pTrig change. In state 0, the absence of a voltage signal keeps FCN(R) reduced, and therefore the pTrig copy number low. In state 1, a +0.5-V signal oxidizes FCN(R) and PMS, which activates the *soxS* promoter to increase the pTrig copy number (Fig. 1c). We observed that the pTrig copy number increased by more than 400-fold

in the presence of the +0.5-V signal (Fig. 1d). Accordingly, newly acquired spacers derived from pTrig were 34 times more prevalent in response to the signal than without, increasing from 0.038(±0.004)% to 1.28(±0.03)% among all arrays in the cell populations (Fig. 1e). Examining the source of newly acquired spacers revealed consistent spacer acquisition across genomic and plasmids regions at each state (Supplementary Fig. 1). These results demonstrate that DRIVES can be wired for direct digital-to-biological encoding in living cells using electronic signals mediated through redox molecules.

Direct encoding of 3-bit digital data into CRISPR arrays. Because spacer acquisition mostly occurs unidirectionally at the 5′ position of the expanding CRISPR array, temporal biological events can be recorded over time[22]. We therefore explored the use of temporal signal induction to encode digital data containing multiple bits in DRIVES as a way to increase the data-storage capacity of a cell population. To scale from 1 bit to 3 bits, we performed an encoding experiment in which cells were exposed to different electrical signal profiles over three sequential rounds, testing all eight possible binary induction combinations (Fig. 2a and Extended Data Fig. 3a,b). The pTrig copy number profiles correlated strongly with the 3-bit binary input profiles associated with each cell population (Fig. 2b and Extended Data Fig. 3c). We also observed an increase in CRISPR array expansion over the course of the experiment (Extended Data Fig. 3d) and an increase in the proportion of pTrig-derived spacers as a function of number of electronic signals (Extended Data Fig. 3e).
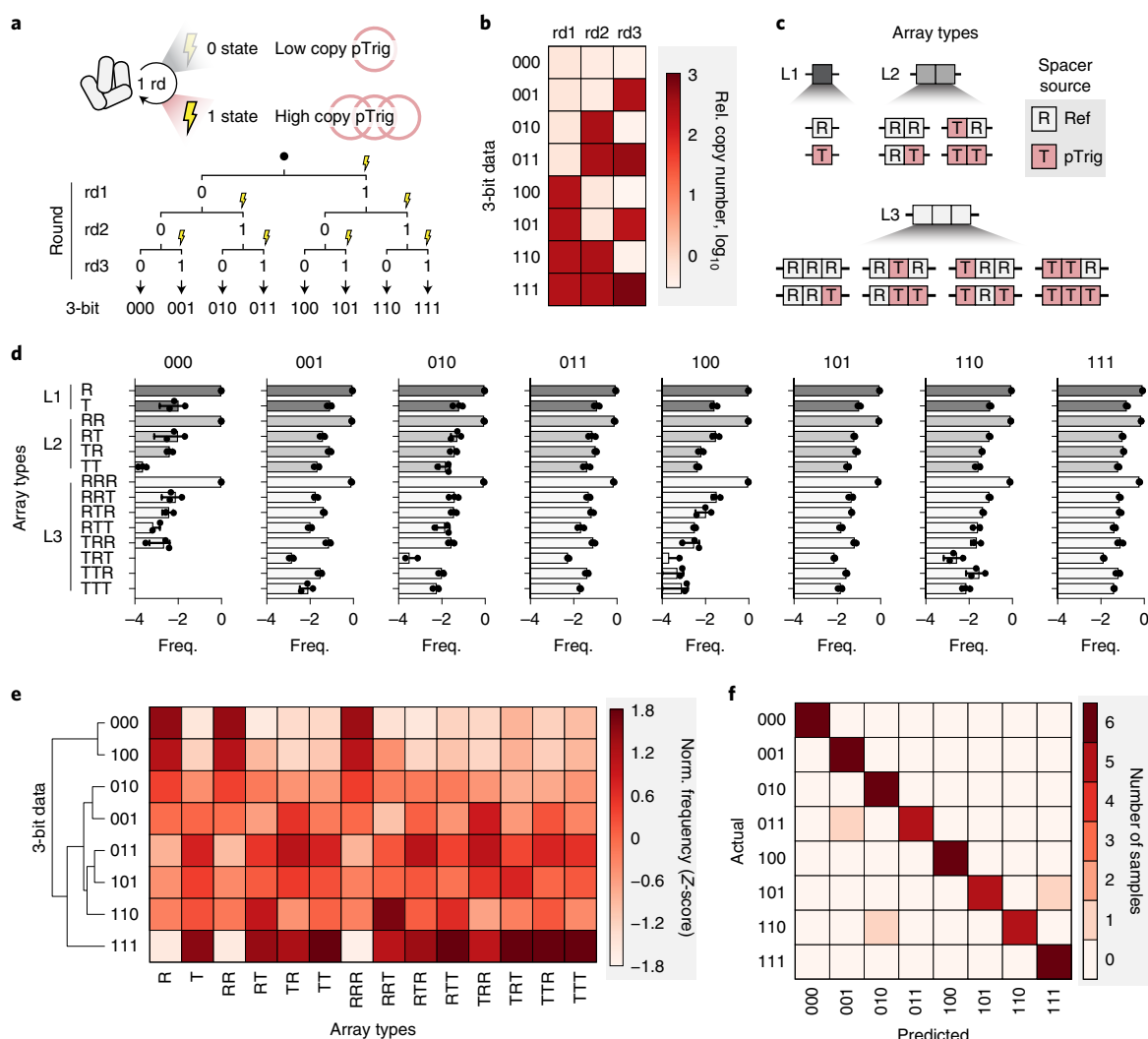
Fig. 2 | Encoding 3-bit binary data into *Escherichia coli* populations. a, Cells were subjected to electrical signals over three sequential rounds, constituting all eight possible 3-bit binary data profiles. **b**, pTrig copy number profiles for each round of the 3-bit binary data profiles. **c**, CRISPR array populations can be described as a frequency distribution constituting of all permutations of reference spacers (R, grey) derived from the genome or pRec and trigger spacers (T, red) derived from pTrig for a given array length (L). **d**, Frequencies of array types in $\log_{10}$ scale for each array lengths for the 3-bit data-encoded CRISPR array populations. **e**, Clustering CRISPR arrays based on their array-type frequency profiles normalized to Z-score across all 3-bit binary profiles. **f**, Performance of a random forest classifier trained on data from three independent experiments and tested on data from six subsequent independent experiments. For classification of each sample, an average of 172,788 total sequencing reads with 89,928 reads of expanded arrays (or 38,295 of L2/L3 arrays) that uniquely map spacers were used. Bead-based size enrichment was performed to enrich for expanded arrays and deplete unexpanded arrays (Methods). All measurements are based on three or more biological replicates. Error bars represent the s.d. of three biological replicates.

To better delineate the data structure of the eight different 3-bit binary data stored in DRIVES, we enriched longer arrays containing more temporal information (Extended Data Fig. 3f) and categorized the observed individual CRISPR arrays in a cell population as a distribution of array types consisting of either reference (genome- or pRec-derived) or trigger (pTrig-derived) spacers at each positions of an observed array length[22] (Methods and Fig. 2c,d). We investigated whether these array-type frequencies could differentiate between different input signal profiles of different cell population by clustering the normalized array-type frequencies (Fig. 2e). Principal component analysis (PCA) on the array-type frequencies revealed eight distinct clusters that differentiated the 3-bit binary data profiles from each other, although there were some overlaps between the clusters (Extended Data Fig. 3g). Application of our previous classification approach[22] using the Euclidean distance between observed and predicted (or reference) array-type frequencies failed

to return reliable classification results (64.6%) on the test datasets (Supplementary Fig. 2). We suspect that the minimal medium contributed to a weaker pTrig copy number induction and thus a lower array expansion efficiency with pTrig-derived spacers. In turn, the array-type frequencies are more biased towards 'R', 'RR' and 'RRR', which limited the ability of other array types to contribute to the Euclidean distance metric (Supplementary Fig. 2a). On the other hand, a supervised learning approach might better account for these limitations as well as pleiotropic host responses induced by strong redox stress from electrical stimulations that may introduce variability across datasets[34] (Extended Data Fig. 3g).

To leverage the unique patterns of the array-type frequencies, we therefore built classifiers to distinguish the observed CRISPR array data to predict the initial signal profile. From three independent experiments that measured all 3-bit profiles, we first trained a random forest classifier on two randomly selected datasets and

tested the model performance on the left-out dataset using L2 and L3 array types. This initial model yielded an accuracy of 87.5% in profile classification (compared to 12.5% by chance) with 10 iterations of repeated random-subsampling and validation (Extended Data Fig. 4a). Encouraged by these initial classification results, we then retrained the model on all three datasets and then tested its performance on newly acquired datasets from six additional independent experiments. This model produced 93.75% accuracy (45 correct classifications out of 48 tested samples) (Fig. 2f), with the 'TRT' array-type frequency as the leading feature for classification (Extended Data Fig. 4b). Approximately 10,000 expanded arrays with uniquely mapping spacers (with ~4,000 L2/L3 arrays) from ~17,000 sequencing reads on size-enriched arrays were sufficient to achieve reasonable classification accuracy (that is, >90%; Extended Data Fig. 4c). The number of reads corresponds to ~200,000 cells in the original data-encoded cell population. Using more datasets for training marginally improved the model performance (Extended Data Fig. 4d). Taken together, these results demonstrate that multi-bit digital data can be stored in electrogenetically actuated CRISPR arrays and the resulting array-type frequencies can be used to recover the stored data from the population.

Scaling data-storage capacity with barcoded arrays. To further extend the data-storage capacity of DRIVES, we sought to devise a multiplexing strategy to write larger-sized binary data across multiple barcoded cell populations in parallel (Fig. 3a). We first generated a library of CRISPR arrays by mutagenizing the distal 8-bp region of the first direct repeat (DR) sequence (Extended Data Fig. 5a), where we previously showed CRISPR arrays could be barcoded[22]. However, many of the DR variants (72%) exhibited notably lower spacer acquisition rates (that is, 50% less than that of wild-type DR; Extended Data Fig. 5b–d), probably due to disrupted interactions between the Cas1–Cas2 complex and the inverted repeats within the first DR sequence at the barcoded region[35]. We then explored introducing the 8-bp barcode downstream of the first spacer in the CRISPR array. Encouragingly, spacer acquisition efficiencies were consistently high across 24 unique spacer-barcoded variants (Extended Data Fig. 5b,c and Supplementary Table 1). We further assessed CRISPR array expansion for different barcoded cells either individually or as a mixed pool and confirmed that pooling barcoded populations does not significantly affect CRISPR expansion measurements in a multiplex format (Extended Data Fig. 5e). Notably, the pooled arrays could be demultiplexed easily into their associated barcodes through a streamlined Illumina sequencing pipeline that uses each barcode also as a sample index. Barcoding the downstream region of the first spacer also enabled targeted extraction of encoded data belonging to specific barcodes from a mixed population (Supplementary Fig. 3), which was not possible in the previous DR barcoding approach. In addition, we performed projections on the scale of DRIVES as a function of Cas1–Cas2 activity, the number of barcodes and sampling depth (Extended Data Fig. 6). These results demonstrate that this new barcoding strategy can yield active CRISPR array variants with high spacer acquisition efficiencies that can be pooled, thus providing a foundation to scale up DRIVES.

Accurate encoding of text directly into living cells. Having established a robust strategy to expand the data storage capacity of DRIVES, we then set out to test the encoding of meaningful information (for example, a text message) into living cells. To transform text messages into binary code, we utilized an encoding strategy where each 'byte' maps to a 6-bit character code (for 2^6 or 64 possible characters) built from two concatenated 3-bit data units over two barcoded cell populations (Fig. 3b). Because our classifier performance was not equal across all 3-bit data profiles (Fig. 2f and Extended Data Fig. 7a), we examined different encoding schemes to optimize character-to-byte mapping (Extended Data Fig. 7b). Two

schemes were explored: (1) the classic DEC 6-bit encoding table for 64 basic ASCII characters and (2) an optimized (OPT) 6-bit encoding table, designed to take into account the letter usage frequency[36] and classifier decoding performance bias. In the OPT encoding scheme, more frequently used characters (based on letter frequency in English text) are assigned to 6-bit bytes with higher decoding performance (Extended Data Fig. 7c). Therefore, OPT encoding was expected to generally outperform DEC encoding for text messages (Extended Data Fig. 7d).

To test the performance of these encoding schemes, we encoded a 12-byte text message, 'hello world!', using either the DEC or OPT table, directly into *E. coli* cells. For each encoding experiment, the text was split into 12 individual 6-bit characters, with each assigned to two barcoded cell populations holding 3-bit data each (Fig. 3b). All 24 barcoded populations were temporally induced with their assigned 3-bit signals in parallel on the multi-channel electrochemical redox controller set-up (Extended Data Fig. 2). During the course of encoding, pTrig copy number profiles exactly matched the binary input profiles for each barcoded population (Fig. 3c). On completion of encoding, the resulting 24 cell populations were pooled and stored at −80 °C as a glycerol stock for subsequent analysis by sequencing. From the sequenced spacers, we determined the array-type frequency profiles from these barcoded populations, which were then classified using our pre-trained random forest model (Fig. 2). Decoding the data from OPT-encoded cells successfully returned the original message 'hello world!' (Fig. 3c). On the other hand, decoding from DEC-encoded cells returned 'xello world!', due to misclassification of the first 3-bit '101' as '111' (Supplementary Fig. 4). We further examined how the data recovery rate depended on the amount of sequencing reads. For the OPT-encoded data, only 1,600 expanded arrays with uniquely mapping spacers for each barcoded cell population (with ~1,000 L2/L3 arrays) from ~2,600 sequencing reads on size-enriched arrays were sufficient to correctly classify ~98% of the 72 bits in the data (Extended Data Fig. 8).

Even with OPT encoding, where errors are intentionally suppressed toward the least frequently used characters (bottom 14%), this encoding scheme can still suffer from non-negligible error rates (average 12.13%; Extended Data Fig. 7c). As shown with the DEC-encoded example, a single-bit error can drastically deteriorate message outcome (Supplementary Fig. 4). To address this shortcoming, we next implemented an error correction strategy using a simple parity check. Given that the last bit of the binary data (generated most recently in the CRISPR array) is always the most reliable for classification, we utilized the last bit of every 6 bits as a checksum for the previous 5 bits (Fig. 2f and Extended Data Fig. 9a,b). After initial classification of an input, the error correction pipeline counts the number of '1' in the first five classified bits and then expects '0' or '1' for a checksum value at the sixth bit based on the counts (Extended Data Fig. 9c and Supplementary Table 2). When the classified checksum value does not match the expected value, the classifier flags that an error has occurred during classification of the character and the error is then corrected based on the classifier's confusion probability. With this error correction pipeline (OPT2), we can only encode up to 32 curated characters, but with significantly higher data reconstruction performance (Extended Data Fig. 9d,e). We encoded the text 'synbio@cu' using the OPT2 encoding/decoding pipeline into cells and found that 2 out of 54 bits were initially misclassified, but the errors were detected and successfully corrected to return the input message (Extended Data Fig. 9f). Although error correction is still imperfect, the OPT2 strategy significantly reduces error rates to 0.79%, on average. Together, these results demonstrate the ability to encode and store meaningful amounts of information directly into living cells using electrical stimulation alone, and show that careful design of information encoding and error-correction strategies can significantly improve the reconstruction accuracy of stored data.
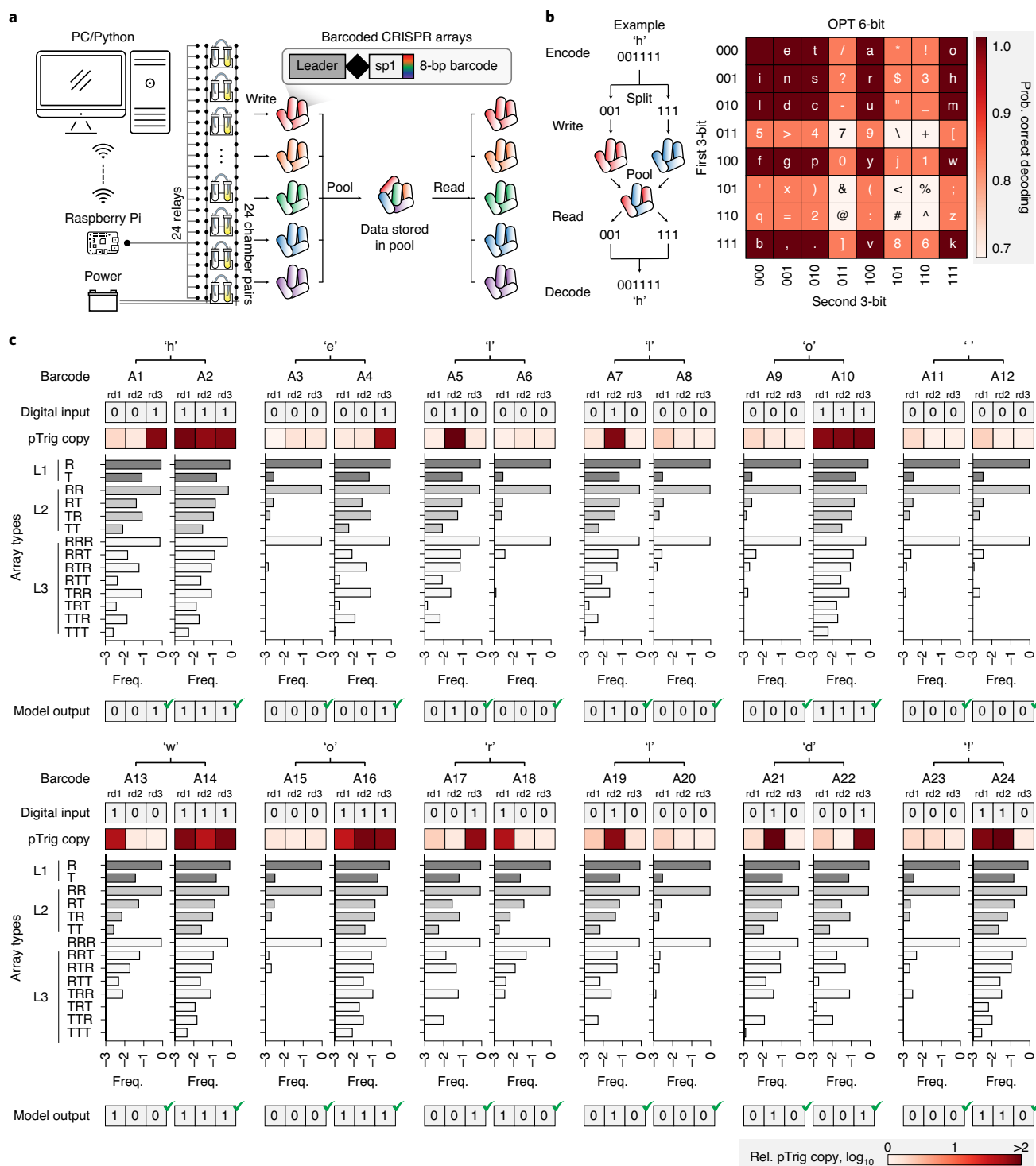
Fig. 3 | Writing the text message 'hello world!' containing 72 bits into barcoded *E. coli* cells. a, Uniquely barcoded cell populations in each chamber on the multi-channel electrochemical redox controller can receive and store 3-bit binary profiles in parallel, split from original data. The 3-bit encoded cells in each chamber can be pooled and stored. Data can be retrieved by sequencing and demultiplexing barcode sequences for data reconstruction. **b**, The optimized (OPT) 6-bit character table that leverages letter usage frequency and retrieval bias. The 6-bit binary data for each character are split into two barcoded cell populations. An example of encoding 'h' is shown. **c**, Array-type frequencies (in $\log_{10}$ scale) from a 'hello world!' encoded cell population. For classification of each barcoded cell population, we used an average of 443,051 total sequencing reads with 271,725 reads of expanded arrays (or 179,174 of L2/L3 arrays) that uniquely map spacers. Bead-based size enrichment was performed to enrich for expanded arrays and deplete unexpanded arrays (Methods). All measurements are based on a single encoding experiment.

Stability of data in replicating cells. Mutations during DNA replication, genomic recombination or changes in cellular fitness could all, in theory, compromise the fidelity of DNA-based data storage in cells. We expect the *E. coli* BL21 genomic CRISPR arrays (where data are stored) to have neutral cellular fitness because the CRISPR interference machineries are absent and we have previously shown
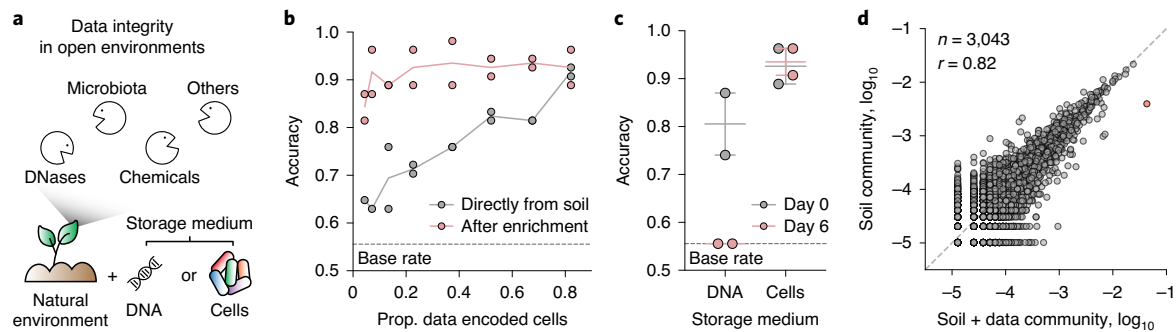
Fig. 4 | Cell envelope as a physical barrier to protect data. a, A data-encoded cell population or naked genomic DNA extracted from the same amount of data-encoded population was challenged to a natural soil environment. **b**, Retrieval of a text message ('synbio@cu') from a mixed microbial community of data-encoded *E. coli* cells and natural soil microbiota with and without selective growth enrichment. Accuracy is defined as the proportion of bits that are correctly classified. For classification of each barcoded cell population, an average of 41,740 total sequencing reads with 20,811 reads of expanded arrays (or 9,821 of L2/L3 arrays) that uniquely map spacers were used. Bead-based size enrichment was performed to enrich for expanded arrays and deplete unexpanded arrays. **c**, Retrieval of the text message 'synbio@cu' stored in naked DNA or in encoded cells after exposure to soil for 0 or 6 days. Accuracy is defined as the proportion of bits that are correctly classified. The plot displays the mean values and whiskers span the highest and lowest points. For classification of each barcoded cell population, an average of 20,542 total sequencing reads with 7,868 reads of expanded arrays (or 2,692 of L2/L3 arrays) that uniquely map spacers were used. Bead-based size enrichment was performed to enrich for expanded arrays and deplete unexpanded arrays. **d**, Comparison of microbial compositions of a natural soil community with and without hidden data-encoded *E. coli* cells (the *Escherichia*/*Shigella* genus is shown in red, 4% spiked-in). OTUs (*n*) and Pearson correlation coefficient (*r*) are shown. The dashed line represents *y* = *x*. All measurements are based on two biological replicates.

that the spacers in CRISPR arrays are stable over 50 generations[22]. Nevertheless, the non-negligible off-target spacer integration rates of the Cas1–Cas2 complex[37] and the continuous growth of the pooled population may lead to subtle changes in subpopulations that become magnified over time to a level at which they may affect data recovery. To assess the stability of stored digital information within an actively dividing bacterial population, we propagated a cell population containing the OPT-encoded data 'hello world!' for over 16 days (~100 generations) and sampled the population at multiple time points throughout (Extended Data Fig. 10). Although data retrieval efficiency gradually decreased with increasing population generations, we found that the data could still be robustly decoded with >90% accuracy from the population for ~80 generations. The drop in data retrieval efficiency is probably due to fluctuations in the population, because the relative abundance of the 24 barcoded subpopulations was stable for ~60 generations before a notable change was observed, suggesting adaptive mutations with fitness effects arising in some of the subpopulation. We further tracked the population in higher resolution using array-type frequencies within each of the barcoded cell populations where encoded information is embedded (Supplementary Fig. 5). Although 15 out of 24 barcoded cell populations (62.5%) in the pool stably maintained the data, the array-type frequencies within the remaining nine barcoded populations gradually shifted, losing their initially encoded information over time. Nevertheless, a >90% accuracy achieved over ~80 generations highlights that data with 72 bits encoded in living cells can be exponentially and autonomously amplified over 80 iterations to yield ~1.2×10^{24} (2^{80}) times more physical copies that can still be robustly decoded.

Integrity of data in natural open environments. The stability and accessibility of DNA are key advantages in data storage[4]. However, there has been limited direct assessment of the fidelity of DNA-based digital information stored in open natural environments, where DNA encounter various degradative factors including DNase enzymes, microorganisms, ultraviolet (UV) light and chemical mutagens (Fig. 4a). To investigate the integrity of data stored in cells in a natural environment, we took a cell population that encoded a text 'synbio@cu' with 54 bits using OPT2 (Extended

Data Fig. 9) and challenged it to commercially purchased organic potting soil at concentrations of 10^7–10^9 cells per 100 mg of soil. Encouragingly, we could retrieve up to 90% of the data from the data-encoded cells in soil at the highest spike-in ratio (82% of the mixed soil microbial community). However, the decoding accuracy decreased when lower proportions of data-encoded cells were present in the mixed community, probably due to missing data from rare array types (Fig. 4b). To address this, we selectively grew the data-encoded subpopulation from the mixed soil microbial community using lysogeny broth (LB) medium supplemented with kanamycin and chloramphenicol, to which data-encoded cells are resistant. Efficient enrichment of data-encoded cells yielded >90% accuracy in data reconstruction for spike-in ratios as low as 7%. We further assessed the stability of the data either in cells or in naked DNA in soil over time. In contrast to naked DNA added directly to soil, where most of the data degraded during a six-day incubation period, data stored in cells were robustly protected and could be decoded without any loss of information (Fig. 4c). In addition, beyond the intrinsic layers of data security used to protect the information embedded within cells (for example, CRISPR array locus, encoding table and so on), we further envisioned the utility of camouflaging encoded data in a natural microbial community with vast biodiversity and sequence complexity. Metagenomic 16S rRNA sequencing of the mixed soil microbiome revealed diverse taxa (4,083 operational taxonomic unit (OTUs)), including the data-encoded *Escherichia*/*Shigella* genus (Supplementary Fig. 6). Natural soil communities with and without hidden data-encoded *E. coli* cells (4% spike-in ratio) showed highly similar microbial compositions, with Pearson's *r* > 0.8 (Fig. 4d), supporting the idea of data concealment in an open setting. Together, these results highlight the relevance of data storage in living cells for protection from natural environments and future steganographic approaches for embedding synthetic data in complex microbiomes.

Discussion

DNA has great potential to become a next-generation data-storage medium. Although recent DNA-storage efforts have advanced nucleic acid synthesis, manipulation and sequencing methods, we focused in this study on developing an all in vivo framework for

digital-to-biological data encoding directly into the genomes of living cells in a single step. We demonstrated scaling of the data storage capacity of DRIVES in two different dimensions: (1) binary data in units of multiple bits by using temporal electronic signals (that is, from 1 bit to 3 bits, with eight possible states) and (2) multiplex encoding across many barcoded cell populations (that is, from 3 bits to 72 bits, with 2^{72} possible states). These strategies can be applied to directly write text messages and the stored data can be reliably recovered and physically amplified through multi-generational growth. Furthermore, data can be hidden within a natural microbial community to enable an additional layer of data security by obscurity. Finally, digital data encoded in the genomes of living cells are protected from harsh natural environments where raw DNA would otherwise be damaged or degraded.

With sufficient sequencing depth and read lengths, the data storage capacity in a cell population is, in principle, governed by the CRISPR array expansion efficiency, the number of barcodes and the population size, and will require further advancements for practical utility (Extended Data Fig. 6). We chose to use a 3-bit storage unit per barcoded cell population in this study, due mostly to a low abundance ($0.173 \pm 0.065\%$) of L3 arrays after three rounds of temporal signal induction. In theory, these rare cells with longer CRISPR arrays contain the most amount of temporal information, but would require larger population sizes to generate at sufficient levels and with deeper sequencing coverages (or amplicon size enrichment) for reliable data reconstruction. The current data storage capacity of DRIVES if scaled suggests that more than 5,000 barcoded cell populations could, in theory, be pooled and decoded using a single Illumina MiSeq sequencing run (Extended Data Fig. 8). Data storage with thousands of barcoded cell populations will require more sophisticated design of multiplexed electrochemical induction set-ups that leverage microplate, on-chip or microfluidic formats[30,38]. Other multiplexable induction modalities such as with light or by acoustics could further increase encoding channel capacity across cell populations[39,40]. We anticipate that improving the CRISPR spacer acquisition system will enable encoding with higher bit units, a faster rate of encoding and better reconstruction from a smaller cell population size. Metagenomic mining of Cas1–Cas2 orthologs[41] and directed evolution[42,43] to improve the CRISPR adaptation machinery or other related host factors are promising paths. Other CRISPR-Cas systems with shorter spacer and DR would enable more compact and denser data storage in CRISPR arrays[44]. Employing more efficient size-enrichment methods and long-read sequencing technologies to decode longer arrays would also improve the overall approach.

Although data-encoded cells could be passaged for over 80 cell generations and still allow robust data recovery at >90% accuracy, we observed mutations arising over time that altered the relative abundance of subpopulations, which led to loss of some array types and deterioration of data fidelity. Engineering host strains with lower mutation rates or other biocontainment strategies could reduce these undesired outcomes[45,46]. Reducing batch-to-batch variability induced by redox-translated electronic signals could improve the reliability of data recovery[34]. Lyophilization or use of spore-forming bacteria could also extend shelf-life for long-term DNA-based data storage[47]. This digital-to-biological data storage framework could be applied to other microbial systems with unique properties such as native electroactivity[48], fast growth[49] or extremo-tolerance[50]. We anticipate that the technical advances described here can provide a foundation for higher-performance DNA-based cellular memory devices used not only in digital data storage but also in other biological recording applications.

Online content

Any methods, additional references, Nature Research reporting summaries, source data, extended data, supplementary information, acknowledgements, peer review information; details of author contributions and competing interests; and statements of data and code availability are available at https://doi.org/10.1038/s41589-020-00711-4.

References

1. Church, G. M., Gao, Y. & Kosuri, S. Next-generation digital information storage in DNA. *Science* **337**, 1628 (2012).
2. Erlich, Y. & Zielinski, D. DNA fountain enables a robust and efficient storage architecture. *Science* **355**, 950–954 (2017).
3. Allentoft, M. E. et al. The half-life of DNA in bone: measuring decay kinetics in 158 dated fossils. *Proc. Biol. Sci.* **279**, 4724–4733 (2012).
4. Ceze, L., Nivala, J. & Strauss, K. Molecular digital data storage using DNA. *Nat. Rev. Genet.* **20**, 456–466 (2019).
5. Newman, S. et al. High density DNA data storage library via dehydration with digital microfluidic retrieval. *Nat. Commun.* **10**, 1706 (2019).
6. Organick, L. et al. Random access in large-scale DNA data storage. *Nat. Biotechnol.* **36**, 242–248 (2018).
7. Anavy, L., Vaknin, I., Atar, O., Amit, R. & Yakhini, Z. Data storage in DNA with fewer synthesis cycles using composite DNA letters. *Nat. Biotechnol.* **37**, 1229–1236 (2019).
8. Lee, H. H., Kalhor, R., Goela, N., Bolot, J. & Church, G. M. Terminator-free template-independent enzymatic DNA synthesis for digital information storage. *Nat. Commun.* **10**, 2383 (2019).
9. Farzadfard, F. & Lu, T. K. Emerging applications for DNA writers and molecular recorders. *Science* **361**, 870–875 (2018).
10. Sheth, R. U. & Wang, H. H. DNA-based memory devices for recording cellular events. *Nat. Rev. Genet.* **19**, 718–732 (2018).
11. Chan, M. M. et al. Molecular recording of mammalian embryogenesis. *Nature* **570**, 77–82 (2019).
12. Kalhor, R. et al. Developmental barcoding of whole mouse via homing CRISPR. *Science* **361**, eaat9804 (2018).
13. McKenna, A. et al. Whole-organism lineage tracing by combinatorial and cumulative genome editing. *Science* **353**, aaf7907 (2016).
14. Munck, C., Sheth, R. U., Freedberg, D. E. & Wang, H. H. Recording mobile DNA in the gut microbiota using an *Escherichia coli* CRISPR-Cas spacer acquisition platform. *Nat. Commun.* **11**, 95 (2020).
15. Farzadfard, F. & Lu, T. K. Genomically encoded analog memory with precise in vivo DNA writing in living cell populations. *Science* **346**, 1256272 (2014).
16. Loveless, T. B. et al. DNA writing at a single genomic site enables lineage tracing and analog recording in mammalian cells. Preprint at *bioRxiv* https://doi.org/10.1101/639120 (2019).
17. Schmidt, F., Cherepkova, M. Y. & Platt, R. J. Transcriptional recording by CRISPR spacer acquisition from RNA. *Nature* **562**, 380–385 (2018).
18. Tang, W. & Liu, D. R. Rewritable multi-event analog recording in bacterial and mammalian cells. *Science* **360**, eaap8992 (2018).
19. Yang, L. et al. Permanent genetic memory with >1-byte capacity. *Nat. Methods* **11**, 1261–1266 (2014).
20. Mimee, M., Tucker, A. C., Voigt, C. A. & Lu, T. K. Programming a human commensal bacterium, *Bacteroides thetaiotaomicron*, to sense and respond to stimuli in the murine gut microbiota. *Cell Syst.* **1**, 62–71 (2015).
21. Riglar, D. T. et al. Engineered bacteria can function in the mammalian gut long-term as live diagnostics of inflammation. *Nat. Biotechnol.* **35**, 653–658 (2017).
22. Sheth, R. U., Yim, S. S., Wu, F. L. & Wang, H. H. Multiplex recording of cellular events over time on CRISPR biological tape. *Science* **358**, 1457–1461 (2017).
23. Roquet, N., Soleimany, A. P., Ferris, A. C., Aaronson, S. & Lu, T. K. Synthetic recombinase-based state machines in living cells. *Science* **353**, aad8559 (2016).
24. Farzadfard, F. et al. Single-nucleotide-resolution computing and memory in living cells. *Mol. Cell* **75**, 769–780 (2019).
25. Akhmetov, A., Ellington, A. D. & Marcotte, E. M. A highly parallel strategy for storage of digital information in living cells. *BMC Biotechnol.* **18**, 64 (2018).
26. Shipman, S. L., Nivala, J., Macklis, J. D. & Church, G. M. CRISPR-Cas encoding of a digital movie into the genomes of a population of living bacteria. *Nature* **547**, 345–349 (2017).
27. Liu, Y. et al. Connecting biology to electronics: molecular communication via redox modality. *Adv. Healthc. Mater.* **6** (2017); https://doi.org/10.1002/adhm.201700789
28. Mimee, M. et al. An ingestible bacterial-electronic system to monitor gastrointestinal health. *Science* **360**, 915–918 (2018).
29. Weber, W. et al. A synthetic mammalian electro-genetic transcription circuit. *Nucleic Acids Res.* **37**, e33 (2009).

30. Bellin, D. L. et al. Electrochemical camera chip for simultaneous imaging of multiple metabolites in biofilms. *Nat. Commun.* **7**, 10535 (2016).

31. VanArsdale, E. et al. A co-culture based tyrosine-tyrosinase electrochemical gene circuit for connecting cellular communication with electronic networks. *ACS Synth. Biol* **9**, 1117–1128 (2020).

32. Gordonov, T. et al. Electronic modulation of biochemical signal generation. *Nat. Nanotechnol.* **9**, 605–610 (2014).

33. Tschirhart, T. et al. Electronic control of gene expression and cell behaviour in *Escherichia coli* through redox signalling. *Nat. Commun.* **8**, 14030 (2017).

34. Bhokisham, N. et al. A redox-based electrogenetic CRISPR system to connect with and control biological information networks. *Nat. Commun.* **11**, 2427 (2020).

35. Nunez, J. K., Lee, A. S., Engelman, A. & Doudna, J. A. Integrase-mediated spacer acquisition during CRISPR-Cas adaptive immunity. *Nature* **519**, 193–198 (2015).

36. Michel, J. B. et al. Quantitative analysis of culture using millions of digitized books. *Science* **331**, 176–182 (2011).

37. Nivala, J., Shipman, S. L. & Church, G. M. Spontaneous CRISPR loci generation in vivo by non-canonical spacer integration. *Nat. Microbiol.* **3**, 310–318 (2018).

38. Din, M. O., Martin, A., Razinkov, I., Csicsery, N. & Hasty, J. Interfacing gene circuits with microelectronics through engineered population dynamics. *Sci. Adv.* **6**, eaaz8344 (2020).

39. Fernandez-Rodriguez, J., Moser, F., Song, M. & Voigt, C. A. Engineering RGB color vision into *Escherichia coli*. *Nat. Chem. Biol.* **13**, 706–708 (2017).

40. Piraner, D. I., Abedi, M. H., Moser, B. A., Lee-Gosselin, A. & Shapiro, M. G. Tunable thermal bioswitches for in vivo control of microbial therapeutics. *Nat. Chem. Biol.* **13**, 75–80 (2017).

41. Makarova, K. S. et al. Evolutionary classification of CRISPR-Cas systems: a burst of class 2 and derived variants. *Nat. Rev. Microbiol.* **18**, 67–83 (2020).

42. Heler, R. et al. Mutations in Cas9 enhance the rate of acquisition of viral spacer sequences during the CRISPR-Cas immune response. *Mol. Cell* **65**, 168–175 (2017).

43. Shipman, S. L., Nivala, J., Macklis, J. D. & Church, G. M. Molecular recordings by directed CRISPR spacer acquisition. *Science* **353**, aaf1175 (2016).

44. Wright, A. V. et al. A functional mini-integrase in a two-protein type V-C CRISPR system. *Mol. Cell* **73**, 727–737 (2019).

45. Blazejewski, T., Ho, H.-I. & Wang, H. H. Synthetic sequence entanglement augments stability and containment of genetic information in cells. *Science* **365**, 595–598 (2019).

46. Deatherage, D. E., Leon, D., Rodriguez, A. E., Omar, S. K. & Barrick, J. E. Directed evolution of *Escherichia coli* with lower-than-natural plasmid mutation rates. *Nucleic Acids Res.* **46**, 9236–9250 (2018).

47. Cox, J. P. Long-term data storage in DNA. *Trends Biotechnol.* **19**, 247–250 (2001).

48. Li, F. et al. Modular engineering to increase intracellular NAD (H/$^+$) promotes rate of extracellular electron transfer of *Shewanella oneidensis*. *Nat. Commun.* **9**, 3637 (2018).

49. Lee, H. H. et al. Functional genomics of the rapidly replicating bacterium *Vibrio natriegens* by CRISPRi. *Nat. Microbiol.* **4**, 1105–1113 (2019).

50. Davis, J. et al. In vivo multi-dimensional information-keeping in *Halobacterium salinarum*. Preprint at *bioRxiv* https://doi.org/10.1101/2020.02.14.949925 (2020).

Methods

Electrochemical set-up. The electrochemical set-up was based on the work in ref. [33], with minor modifications (Extended Data Fig. 2). Briefly, 12-cm-long platinum wires (0.5-mm diameter, 99.99% purity) were wound and used for both working and counter electrodes. For agar salt bridges, 12-cm clear PVC tubings (2-mm inner diameter, 4-mm outer diameter) were filled with heated 3% agar with 1 M KCl solution and stored in 3 M KCl at 4 °C. A typical electrochemical set-up procedure for FCN(R/O) conversion and encoding experiments was performed as follows: the working electrode was placed in a 2-ml tube (working chamber) with 1.5 ml of M9 minimal medium supplemented with 100 ng ml⁻¹ anhydrotetracycline (aTc), 1.56 mM ferrocyanide (FCN(R), reduced), 100 μM phenazine methosulfate (PMS), 20 μg ml⁻¹ chloramphenicol and 50 μg ml⁻¹ kanamycin, and the counter electrode was placed in another 2-ml tube (counter chamber) with 1.5 ml of M9 minimal medium supplemented with 1.56 mM ferricyanide (FCN(O), oxidized) and 100 μM PMS, unless otherwise stated. A pair of working and counter chambers were connected by a PVC salt bridge.

Electronic control of recordings. *Escherichia coli* BL21 strain was transformed with pRec and pTrig, modified from our previous work[22] by replacing the *lacI* gene with the *soxR* gene on pRec and the *lac* promoter with the *soxS* promoter on pTrig (Extended Data Fig. 1a). The transformed strain was inoculated into a culture tube with 3 ml of LB medium supplemented with 20 μg ml⁻¹ chloramphenicol, and 50 μg ml⁻¹ kanamycin and grown overnight in a shaking incubator at 37 °C, aerobically. The culture was diluted 1:30 into a new culture tube with 3 ml LB medium supplemented with 20 μg ml⁻¹ chloramphenicol, and 50 μg ml⁻¹ kanamycin and grown for 2 h aerobically to bring the culture into the exponential growth phase. The culture was then moved to an anaerobic chamber and diluted 1:30 into a working chamber prepared as above. For induction by electronic signals, +0.5 V (on, 1) or 0 V (off, 0) was applied to the chamber for 14 h. The solutions in the working and counter chambers were mixed by pipetting every 1–2 h to facilitate electrochemical conversion and gene expression induction. Subsequently, 500 μl of the culture was collected to assess pTrig copy number by quantitative polymerase chain reaction (qPCR). The remaining cell culture was diluted 1:100 into a new culture tube with 3 ml of LB medium supplemented with 20 μg ml⁻¹ chloramphenicol, and 50 μg ml⁻¹ kanamycin and grown overnight aerobically. A 500 μl volume of the cell culture was collected for subsequent analysis of CRISPR arrays for this round of encoding. For multi-round encoding, the remaining cell culture was diluted again into 3 ml of LB medium supplemented with 20 μg ml⁻¹ chloramphenicol, and 50 μg ml⁻¹ kanamycin and other steps were repeated for the next round.

Barcoding of CRISPR arrays. To facilitate CRISPR array barcoding, endogenous CRISPR array I in *E. coli* BL21 genome was removed by homologous recombination using pSim6 plasmid[51]. Both DR barcoding and spacer barcoding were carried out by one-step cloning and an integration protocol based on a bacteriophage integrase[52]. For DR barcoding, the 8 bp of the distal end of the first DR of the minimal CRISPR array (80-bp leader sequence + DR + the first spacer of the original CRISPR array I) was diversified using degenerate oligonucleotides and the barcoded arrays were inserted into the pOSIP-CH backbone plasmid. For spacer barcoding, we added the 8-bp sequence of Illumina i7 indexes to the downstream region of the first spacer of the minimal CRISPR array on the pOSIP-CH backbone plasmid. After integration of the plasmids into the genomes of *E. coli* BL21 strain without endogenous CRISPR array I, the backbone part of the plasmids was excised by introducing pE-FLP plasmid for FLP recombinase expression, which was then removed using a temperature-sensitive replicon. The sequences of the spacer barcoded CRISPR arrays are listed in Supplementary Table 1.

Array sequencing and data analysis. CRISPR arrays were sequenced using our established sequencing pipeline[22] with minor modifications for the barcoded CRISPR arrays. Briefly, cells were lysed using a prepGEM bacteria kit (MicroGEM) for amplification of input CRISPR array sequences from the DNA. After PCR amplification of CRISPR arrays, samples were pooled and, for selected libraries, magnetic bead-based size enrichment was performed using AMPureXP beads (Beckman Coulter A63881) as previously described. Sequencing was performed on the Illumina MiSeq platform (MiSeq v2 300 cycle) with additional spike-in of custom sequencing primers. The primer sequences are listed in Supplementary Table 3. The raw sequencing data were processed using our established CRISPR spacer extraction and mapping pipeline, which is available at https://github.com/ravisheth/trace with minor modifications. Briefly, raw sequencing reads were subjected to spacer extraction (spacer_extraction.py), the extracted spacers were mapped to their sources (blast_search.sh), then uniquely mapping spacers were determined (unique_spacers.py). Further analysis and data visualization were performed mostly in Python with the numpy, scipy, pandas, scikit-learn, matplotlib and seaborn packages. We considered only arrays with uniquely mapping spacers at all positions within the array, determined if each spacer was either from reference (genome or pRec) or trigger (pTrig), and determined the frequency of each array type normalized across all possible combinations for the given array length.

qPCR assay for pTrig copy number. The pTrig copy number of a cell culture was assessed by qPCR. Briefly, 5 μl of 2× KAPA SYBR Fast qPCR master mix, 0.5 μl

of 10 μM forward and reverse primers, 3 μl of nuclease free water and 1 μl of cell lysate prepared using a prepGEM bacteria kit (MicroGEM) were mixed in each well of a 96-well qPCR plate. Two qPCRs were performed to quantify the pTrig and genomic DNA present in each sample. The primer sequences are listed in Supplementary Table 3.

DNA extraction from soil. DNA extraction from soil was performed using our established protocol with a Qiagen MagAttract PowerMicrobiome DNA/RNA Kit (Qiagen 27500-4-EP)[53]. Briefly, 100 mg of soil samples mixed with data-encoded cell population at various ratios was added to the plate. A 200 μl volume of 0.1-mm Zirconia silica beads (BioSpec 11079101Z) and 750 μl of lysis solution (90 ml master mix: 9 ml of 1 M Tris-HCl pH 7.5, 9 ml of 0.5 M EDTA pH 8.0, 11.25 ml of 10% SDS, 22.5 ml of Qiagen lysis reagent, 38.25 ml of nuclease-free water) were added to each well of the plate. The plate was then subjected to bead beating for 2.5 min followed by 7.5 min of cooling on a bead beater (BioSpec 1001). This bead beating cycle was repeated four times. The plate was centrifuged for 5 min at 4,300g and 150 μl of supernatant was transferred to a V-bottom microplate. A 35 μl volume of Qiagen inhibitor removal solution was added and the plate was centrifuged for 5 min at 4,300g, then 100 μl of supernatant was transferred to a round-bottom plate (Corning 3795) on a robotic liquid handler (Biomek 4000) for magnetic bead purification according to the manufacturer's recommendations, but at a scaled volume. The final elute was further diluted 10-fold with nuclease-free water to minimize the effect from any residual PCR inhibitors from soil.

16S rRNA sequencing and data analysis. The V4 region of the 16S rRNA gene was sequenced using our established sequencing pipeline[53]. After PCR amplification of the 16S rRNA V4 regions from the soil DNA, the resulting ~390-bp amplicon was gel-purified and sequenced on the Illumina MiSeq platform (MiSeq v2 300 cycle) with additional spike-in of custom sequencing primers. The sequencing data were processed using USEARCH v11.0.667[54]. Reads were merged (-fastq_mergepairs), filtered (-fastq_filter -fastq_maxee 1.0 -fastq_minlen 240), then error-corrected OTUs (ZOTUs) were generated (-unoise3) and an OTU table was created (-otutab). Taxonomy was assigned to ZOTUs using the RDP classifier[55]. A phylogenetic tree was constructed using The Interactive Tree of Life (https://itol.embl.de)[56].

Reporting Summary. Further information on research design is available in the Nature Research Reporting Summary linked to this Article.

Data availability

All data supporting the findings of this study are available within the Article and its Supplementary Information or are available from the authors upon request. Sequencing data associated with this study are available at NCBI SRA under PRJNA625964.

Code availability

All of the CRISPR spacer extraction and mapping software can be accessed at https://github.com/ravisheth/trace or are available from the authors upon request.

References

51. Sharan, S. K., Thomason, L. C., Kuznetsov, S. G. & Court, D. L. Recombineering: a homologous recombination-based method of genetic engineering. *Nat. Protoc.* **4**, 206–223 (2009).
52. St-Pierre, F. et al. One-step cloning and chromosomal integration of DNA. *ACS Synth. Biol.* **2**, 537–541 (2013).
53. Ji, B. W. et al. Quantifying spatiotemporal variability and noise in absolute microbiota abundances using replicate sampling. *Nat. Methods* **16**, 731–736 (2019).
54. Edgar, R. C. Search and clustering orders of magnitude faster than BLAST. *Bioinformatics* **26**, 2460–2461 (2010).
55. Wang, Q., Garrity, G. M., Tiedje, J. M. & Cole, J. R. Naive Bayesian classifier for rapid assignment of rRNA sequences into the new bacterial taxonomy. *Appl. Environ. Microbiol.* **73**, 5261–5267 (2007).
56. Letunic, I. & Bork, P. Interactive Tree Of Life (iTOL) v4: recent updates and new developments. *Nucleic Acids Res.* **47**, W256–W259 (2019).

Author contributions

S.S.Y., R.U.S and H.H.W. developed the initial concept. S.S.Y. performed experiments and analyzed the results under the supervision of H.H.W. S.S.Y., R.M.M. and A.M.S.

designed and constructed the electrochemical redox controller set-up. S.S.Y. and Y.H. designed the error correction pipeline. S.S.Y. and H.H.W. wrote the mansucript, with input from all authors.

Competing interests

H.H.W. is a scientific advisor to SNIPR Biome. The other authors declare no competing interests.

Additional information

Extended data is available for this paper at https://doi.org/10.1038/s41589-020-00711-4.

Supplementary information is available for this paper at https://doi.org/10.1038/s41589-020-00711-4.

Correspondence and requests for materials should be addressed to H.H.W.

Reprints and permissions information is available at www.nature.com/reprints.
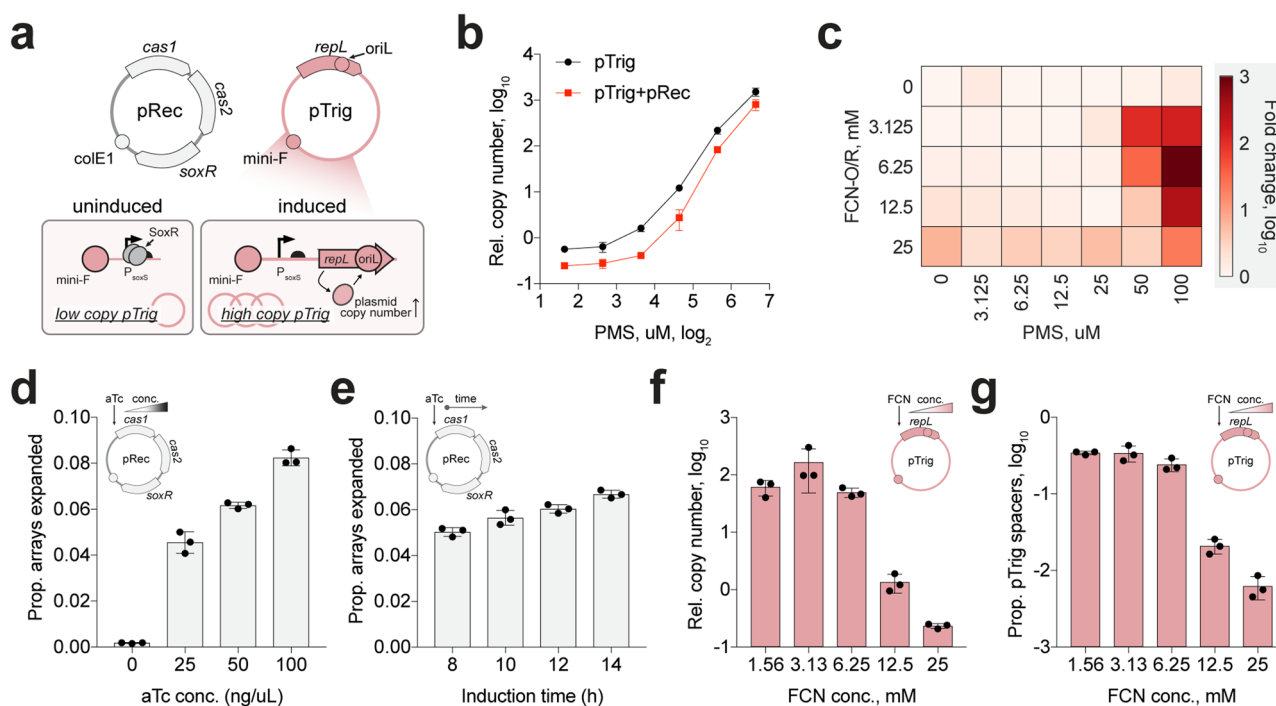
Extended Data Fig. 1 | Development of a redox-sensing DNA-based cellular recorder for direct digital-to-biological data storage. This system is composed of two distinct modules: (i) a 'sensing module' that converts a desired biological signal into a change in copy number of a trigger plasmid (pTrig), and (ii) a 'writing module' that overexpresses Cas1-Cas2 from a recording plasmid (pRec) to unidirectionally expand genomic CRISPR arrays with novel ~33 bp spacers acquired from genomic or plasmid DNA sources in the cell. In the presence of the desired signal, cells experience a shift in their intracellular DNA pool, driven by an increase in pTrig copy number, which results in an acquisition bias for pTrig-derived spacers amongst expanding CRISPR arrays. **a**, The *lacI* gene in the previous pRec[22] was replaced with *soxR* gene from *E. coli*, and the *lac* promoter in the previous pTrig[22] was replaced with *soxS* promoter from *E. coli*. P1 replication system is inactive in the absence of oxidative stress, and a mini-F origin keeps the pTrig plasmid copy number low. Upon induction with oxidative stress, SoxR detaches from *soxS* promoter and activates the P1 replication system to increase the copy number of the plasmid. **b**, pTrig copy number in the presence of various concentrations of phenazine methosulfate (PMS) in aerobic condition. pRec (with an additional copy of *soxR* gene) helps get higher fold-change of pTrig copy number by more efficient repression in absence of the inducer. **c**, pTrig copy numbers in the presence of pRec and various concentrations of PMS, and FCN(R) or FCN(O) in anaerobic condition. Fold change of the pTrig copy numbers at the given concentrations of FCN(R) or FCN(O) were plotted. **d**, Various aTc concentrations and **(e)** induction time for the expression of *cas1* and *cas2* genes were tested for CRISPR array expansion. **f**, Various FCN(R) and FCN(O) concentrations were tested for pTrig copy number induction and **(g)** pTrig-derived spacer incorporation. The proportions of pTrig-derived spacers among all newly incorporated spacers are displayed. All measurements are based on three biological replicates. Error bars represent s.d. of three biological replicates.
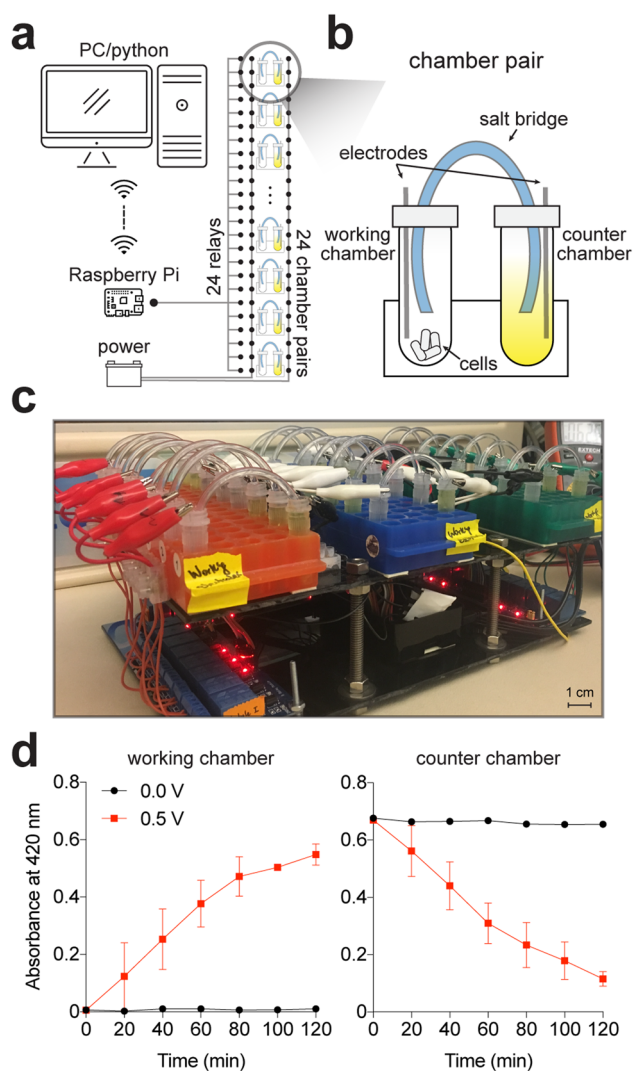
Extended Data Fig. 2 | Construction of a multi-channel electrochemical redox controller. a, In an anaerobic chamber, a Raspberry Pi controls 3 of 8-channel relay modules (total 24 relays), which turn on or off electrical signals into each chamber pair from a power supply, based on a python script running on a wirelessly connected PC. **b**, A pair of working and counter chambers is connected by an agar salt bridge. In a working chamber, cells are incubated in M9 minimal medium supplemented with antibiotics, aTc, FCN(R) and PMS. M9 minimal medium supplemented with FCN(O) and PMS is filled in another chamber (counter). **c**, A photograph of the multi-channel electrochemical redox controller in an anaerobic chamber. **d**, Changes in electrochemical redox states of FCN(R) in a working chamber (left) and FCN(O) in a counter chamber (right) measured by absorbance at 420 nm with (0.5 V) and without (0.0 V) electronic signals. All measurements are based on three replicates. Error bars represent s.d. of three replicates.
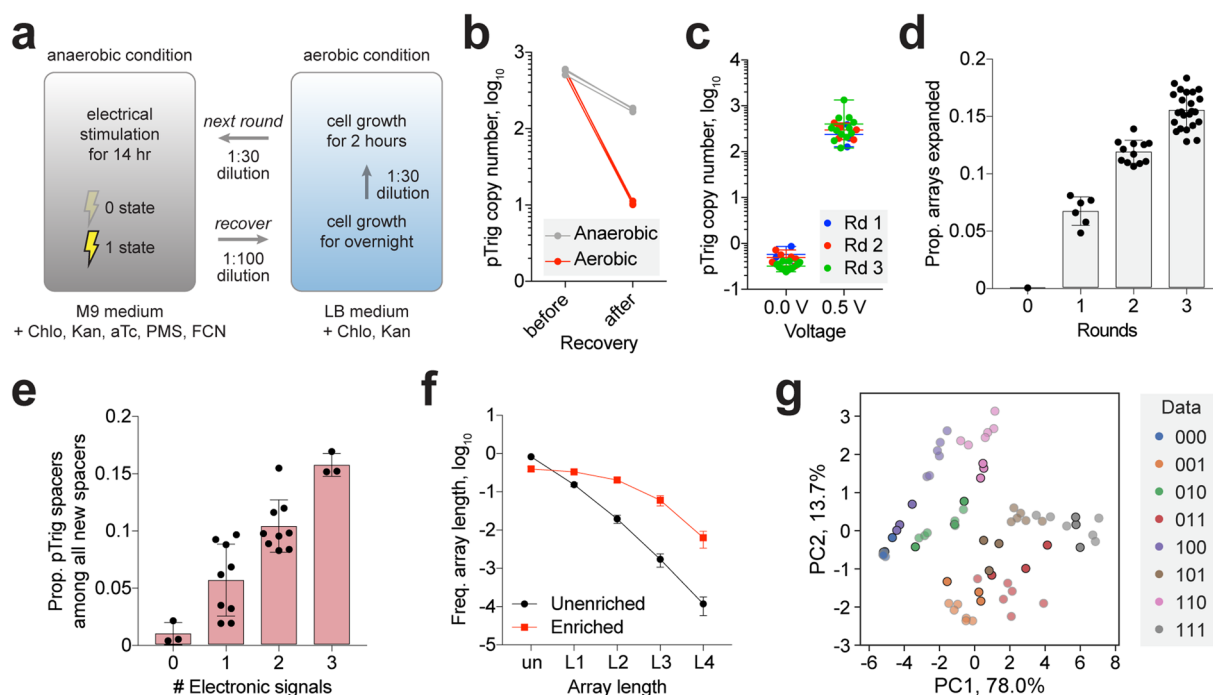
Extended Data Fig. 3 | Encoding of 3-bit binary data profiles. a, Schematic diagram of experimental steps for multi-round encoding. After each round of electrical stimulation, the cell population was recovered in the rich medium (LB) aerobically so that the induced/uninduced plasmid copy number in the previous encoding round can be diluted out and reset low. **b,** To determine the recovery condition, anaerobic and aerobic conditions were compared. **c,** Overlaid distributions of the plasmid copy numbers with/without signals at each round over the course of the multi-round encoding (Fig. 2b). **d,** CRISPR array expansion over the course of the experiment. **e,** The 3-bit binary data profiles are grouped by the number of electronic signals, and the proportions of pTrig-derived spacers among all newly incorporated spacers are displayed. **f,** To enrich the sequencing reads for expanded arrays with more new spacers (longer arrays), the magnetic bead-based size enrichment was performed. Frequency of arrays of different lengths (unexpanded and L1-L4) with and without size enrichment are plotted. **g,** Principal component analysis on the array-type frequency profiles for the 3-bit digital data profiles. All 9 independent biological replicates are shown for each 3-bit digital data profiles. The first three independent datasets used for training of the Random Forest classifier are highlighted. All measurements are based on two or more biological replicates. Error bars represent s.d. of three or more biological replicates.
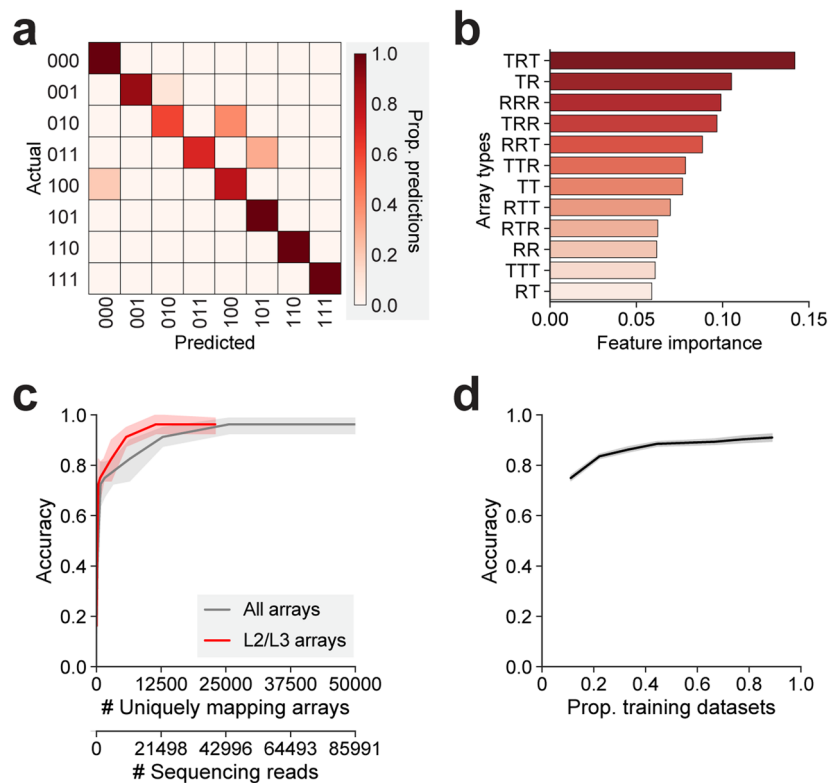
Extended Data Fig. 4 | Performance of a Random Forest classifier for data reconstruction. a, Confusion matrix from cross validation of the Random Forest classifier for 10 times by training on randomly selected 2 datasets for each 3-bit digital data profile from the 3 independent experiments and testing the trained model on the left-out 1 dataset. **b**, Importance of features (array-types) for the Random Forest classifier in Fig. 2f. **c**, Classification performance for the number of CRISPR arrays. CRISPR arrays with new uniquely mapping spacers were randomly subsampled to the various numbers for the 3-bit digital data profiles and classifications were performed. Recall accuracies for distinguishing 8 different types of 3-bit digital data profiles were displayed as a function of the number of expanded arrays with uniquely mapping spacers (grey: all arrays, red: L2/L3 arrays). The number of sequencing reads corresponding to the number of expanded arrays with uniquely mapping spacers (grey: all arrays) is also provided as an additional x-axis. Shaded regions represent 95% confidence interval of 10 iterations of subsampling and classification. **d**, Recall accuracies for distinguishing 8 different types of 3-bit digital data profiles with varying proportions of randomly selected training datasets for each 3-bit digital data profile. Shaded regions represent 95% confidence interval of 100 iterations of subsampling and classification.
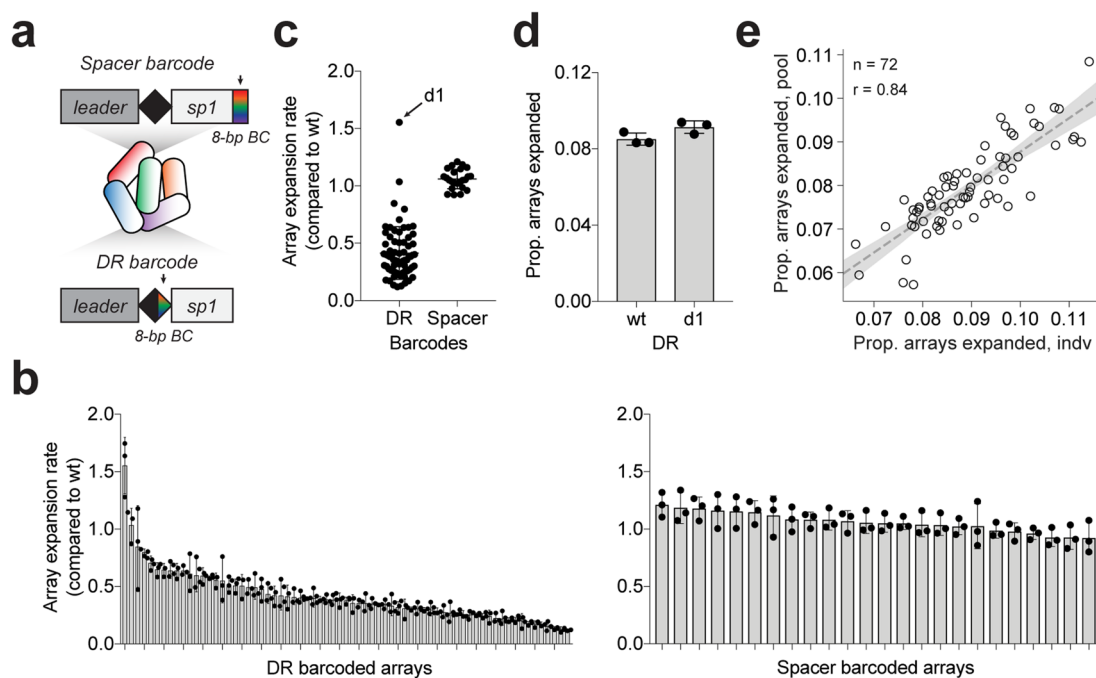
Extended Data Fig. 5 | Barcoding CRISPR arrays for multiplexed encoding. a, CRISPR arrays can be barcoded with 8-bp unique sequences either downstream of the 1st spacer region or within direct repeat (DR) region. **b**, CRISPR array expansion rates (relative to wild-type array) of 69 DR-barcoded CRISPR arrays and 24 spacer-barcoded CRISPR arrays. **c**, Distribution of array expansion rates of spacer-barcoded CRISPR arrays is much more uniform and consistent than that of DR-barcoded CRISPR arrays. A DR variant (d1) that was more efficient than the wild-type DR sequence in the initial 96-well plate-based test is highlighted. **d**, The d1 DR variant was tested again in tube culture condition. In tube culture condition, however, the DR variant did not show significantly higher activity than that of the wild-type DR sequence. **e**, Comparison of CRISPR array expansion rates measured individually or in pool. Shaded region represents 95% confidence interval for linear regression (dashed grey line). Sample sizes (n) and Person correlation coefficient (r) are shown. All measurements are based on three biological replicates. Error bars represent s.d. of three biological replicates.
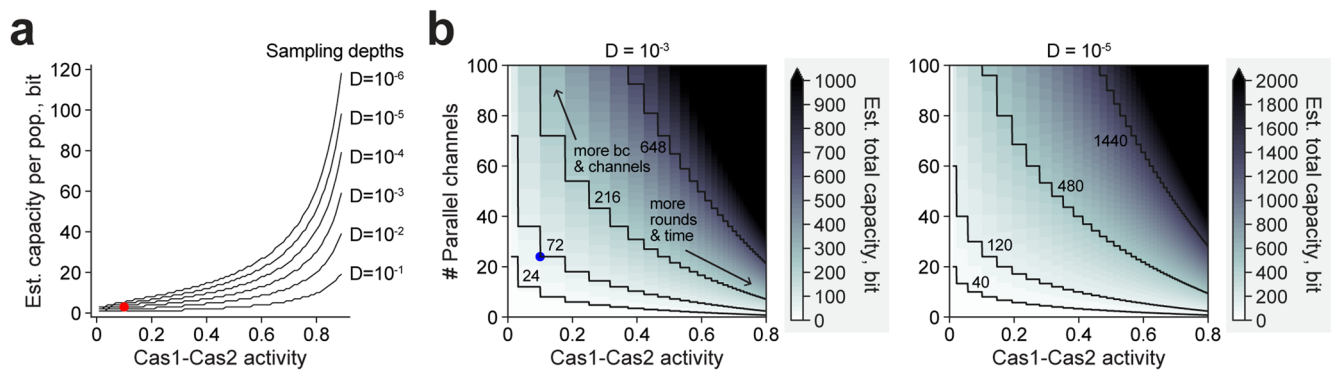
Extended Data Fig. 6 | Projections on the scale of DRIVES. a, Data storage capacity ('n' bits of information or 'n' rounds of encoding) per cell population is estimated as a function of Cas1-Cas2 activity ('X' proportion of the cell population expanded arrays with a new spacer after a single round of encoding). Here, 'X^n' proportion of the cell population would have expanded arrays every round resulting 'n' new spacers (Ln arrays) after 'n' rounds of encoding, and we assumed that the sampling capacity for the Ln array population governs the data storage capacity. We considered various sampling depths 'D', where 'D' proportion of the cell population can be sufficiently sampled. This 'D' could be affected by many factors including the sequencing depth and size enrichment efficiency. We assumed that if the 'X^n' is same or higher than the given sampling depth constraint 'D', 'n' bits can be stored and reliably decoded. For example, when 0.001 of the cell population can be sufficiently sampled (D=0.001), maximum data storage capacity would be 3 bits (n=3) with the current Cas1-Cas2 activity level (X=0.1) as in our current experimental dataset (highlighted in red in the plot). And when 0.0001 of the cell population can be sufficiently sampled (D=0.0001), maximum data storage capacity would be 4 bits (n=4) with the current Cas1-Cas2 activity level (X=0.1). Although the Illumina MiSeq v2 300 cycles kit used in this study can read only up to 5 new spacers, we assumed that sequencing read length is not the limiting factor in this projection as other long read sequencing technologies could be employed. **b**, Estimated total data storage capacity across barcoded cell populations as a function of Cas1-Cas2 activity and the number of parallel channels in the culture platform at two different sampling depths (D=0.001 and D=0.00001). A larger data per cell population would require more rounds of encoding which takes longer time, and a larger number of parallel channels would require more barcoded cell populations and more sophisticated design of the culture platform. Current capacity of the system with 24 channels in the culture platform is highlighted in blue in the plot.
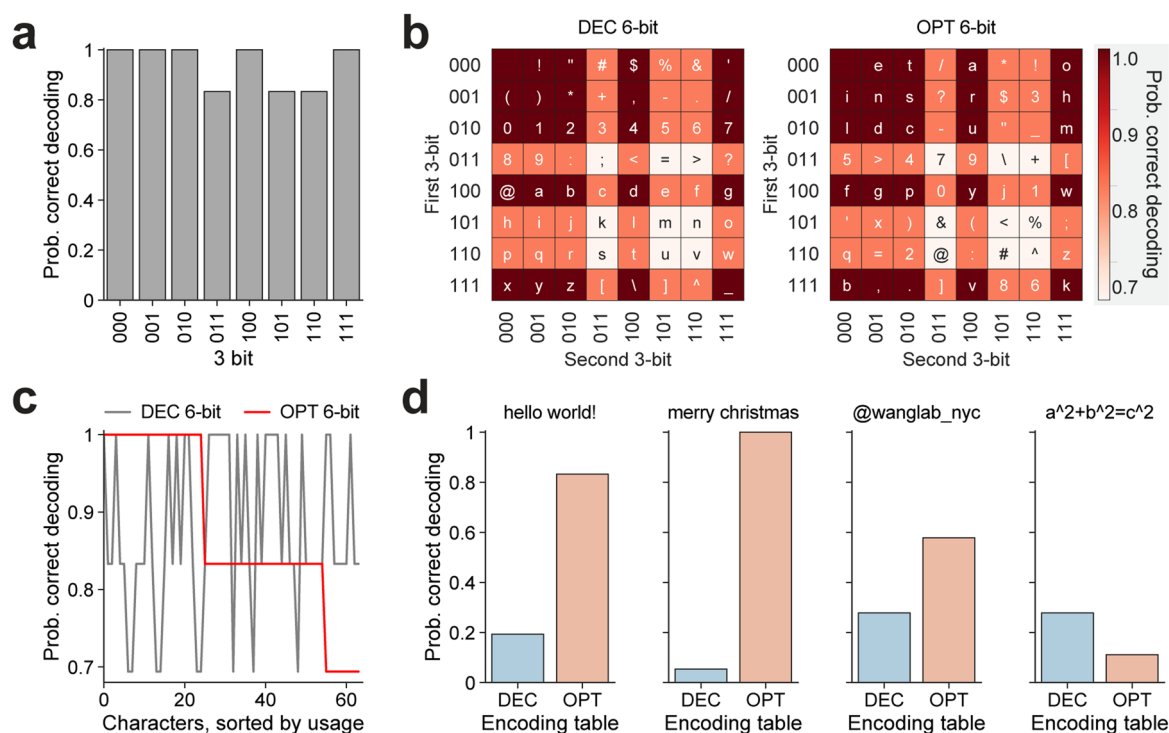
Extended Data Fig. 7 | Design of 6-bit encoding tables for text messages. a, Probability of correct classification for each of the 3-bit digital data profiles by the Random Forest classifier on the newly generated independent datasets is calculated based on the result in Fig. 2f. **b**, DEC and OPT encoding tables with estimated probabilities of correct classification for the 64 characters. OPT 6-bit encoding table was designed by considering the correct classification probability and the usage frequency of the characters (https://mdickens.me/typing/letter_frequency.html). **c**, Probability of correct decoding for the 64 characters (ordered by usage) with DEC and OPT 6-bit encoding tables. **d**, Comparison of predicted probabilities of correct decoding for various text messages based on the two encoding tables. The predicted probabilities of correct decoding for each character or text message were calculated by multiplying the correct decoding probability values of each 3-bit digital data profile units.
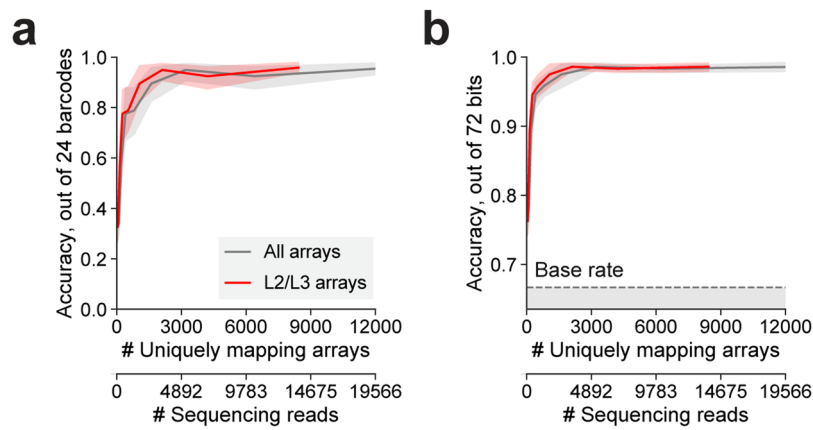
Extended Data Fig. 8 | Reading 'hello world!' from subsampled sequencing reads. Sequencing reads from each barcode in the 'hello world!'-encoded cell population using OPT table were randomly subsampled to the various numbers and classifications were performed. Recall accuracies for **(a)** distinguishing 3-bit digital data profiles for 24 barcoded populations or for **(b)** calling correct bits out of 72 bits were displayed as a function of the number of expanded arrays with uniquely mapping spacers (grey: all arrays, red: L2/L3 arrays). The number of sequencing reads corresponding to the number of expanded arrays with uniquely mapping spacers (grey: all arrays) is also provided as an additional x-axis. Shaded regions represent 95% confidence interval of 10 iterations of subsampling and classification.
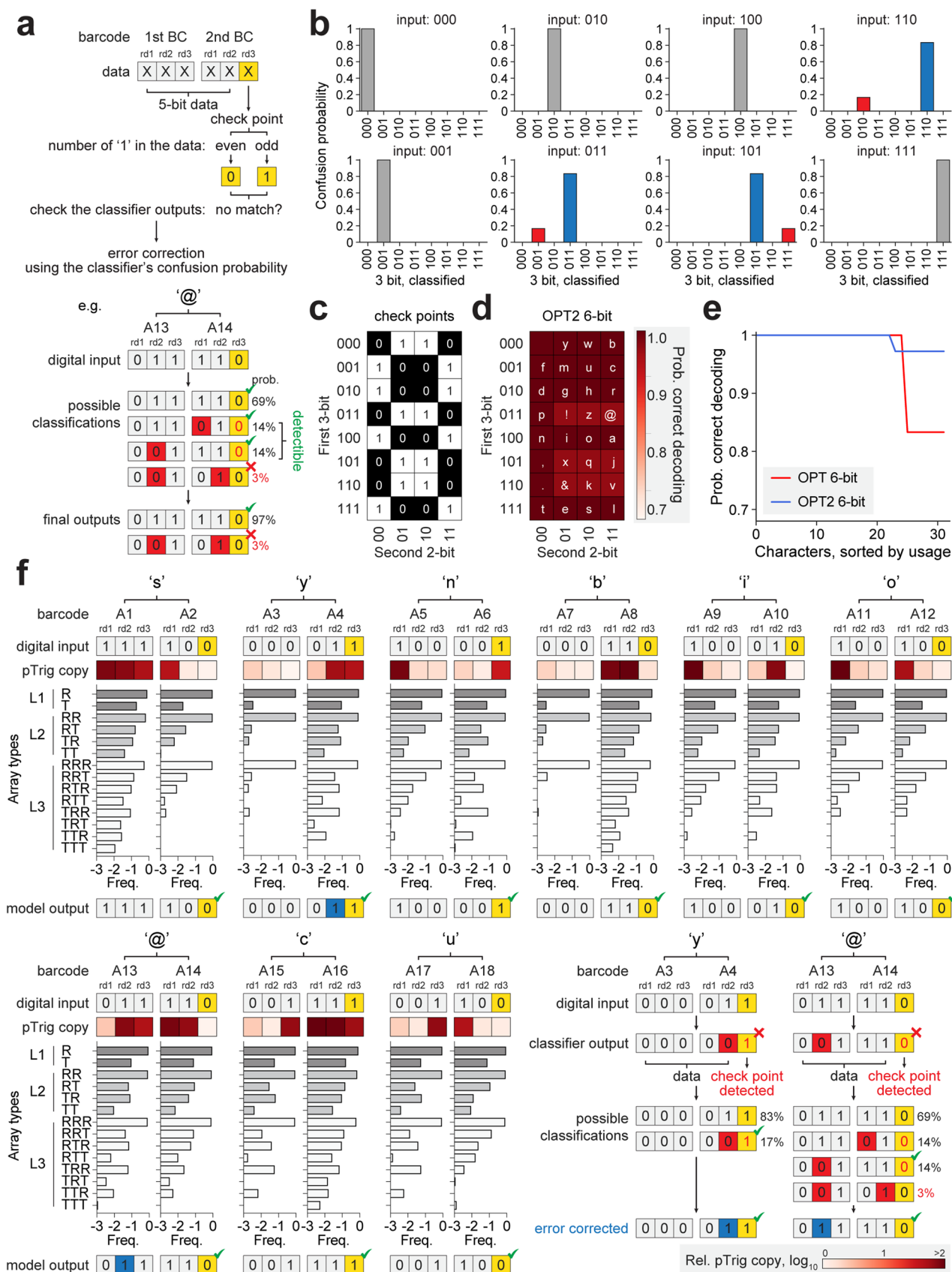
Extended Data Fig. 9 | See next page for caption.

Extended Data Fig. 9 | Improving data reconstruction with error correction. a, By using every sixth bit as a check point (checksum) for the first 5 bits, errors in data reconstruction can be detected and corrected for the selected 32 combinations of 6-bit digital data profiles based on the classifier's confusion probability in Fig. 2f and Extended Data Fig. 9b. For example, for a digital input '011110' could be classified as '011110', '011010', '001110', or '001010' with the probabilities of 69%, 14%, 14%, or 3%, respectively. Out of these 4 possible initial classifications, the last 3 are wrong and the 2 wrong classifications with a single bit error can be detected by the check point values and fixed. However, the classification result with 2 bits error cannot be detected by the check point value and therefore cannot be fixed. For all 32 combinations of 6-bit digital data profiles, possible classification results, their probabilities, and whether they can be fixed or not are summarized in Supplementary Table 2. **b**, Confusion probability for each of the 3-bit digital data profiles based on Fig. 2f. **c**, The check point values for each combination of eight 3-bit and four 2-bit digital data profiles. **d**, OPT2 encoding table with the estimated probabilities of correct classification for the 32 characters. **e**, Probability of correct decoding for the 32 characters (ordered by usage) for OPT and OPT2 6-bit encoding tables. **f**, 'synbio@cu' encoded in the genomes of barcoded *E. coli* populations using the OPT2 error correction strategy. Two errors from the initial classification were detected using the check points and successfully corrected as described in the figure. For classification of each barcoded cell population, an average of 492,289 total sequencing reads with 268,066 reads of expanded arrays (or 106,242 of L2/L3 arrays) that uniquely map spacers were used. Bead-based size enrichment was performed to enrich for expanded arrays and deplete unexpanded arrays. Frequencies of array-types are in $\log_{10}$ scale. All measurements are based on a single experimental study.
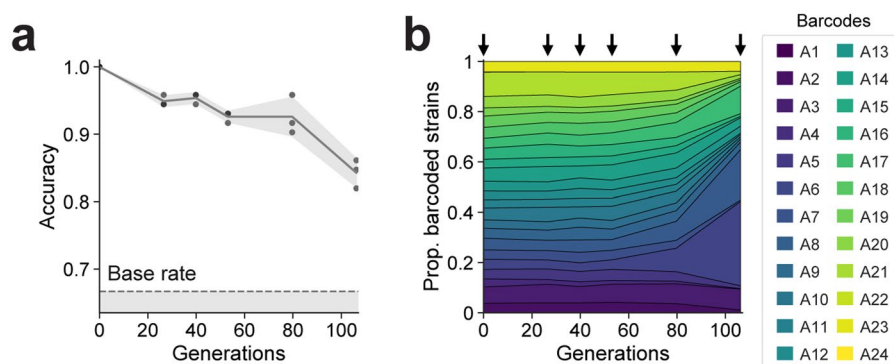
Extended Data Fig. 10 | Data stability in replicating cells. A mixed pool of 24 barcoded cell population encoded with a 72-bit text message 'hello world!' in Fig. 3 was subsequently diluted 1:100 every 24 hours into 3 mL fresh LB media with antibiotic for a total of 16 days (~106 generation, ~6.6 generations per day). **a**, Data stability in the propagating cell population over 100 generations. Accuracy indicates the proportion of bits that are correctly classified. >90% of the 72 bits could be correctly retrieved up to ~80 generations. Shaded region represents s.d. of three biological replicates. For classification of each barcoded cell population, an average of 82,860 of total sequencing reads with 40,502 reads of expanded arrays (or 17,139 of L2/L3 arrays) that uniquely map spacers were used. Bead-based size enrichment was performed to enrich for expanded arrays and deplete unexpanded arrays. **b**, Gradual changes in the relative abundance of 24 barcoded cell population over time suggests adaptive mutations with fitness effects arising in some of the subpopulation. Samples were collected at the time points indicated by arrows (day 0, 4, 6, 8, 12, and 16). All measurements are based on three biological replicates.

Corresponding author(s): Harris H. Wang

Last updated by author(s): Oct 27, 2020

Reporting Summary

Nature Research wishes to improve the reproducibility of the work that we publish. This form provides structure for consistency and transparency in reporting. For further information on Nature Research policies, see our Editorial Policies and the Editorial Policy Checklist.

Statistics

For all statistical analyses, confirm that the following items are present in the figure legend, table legend, main text, or Methods section.

n/a	Confirmed	
☐	☒	The exact sample size (*n*) for each experimental group/condition, given as a discrete number and unit of measurement
☐	☒	A statement on whether measurements were taken from distinct samples or whether the same sample was measured repeatedly
☒	☐	The statistical test(s) used AND whether they are one- or two-sided *Only common tests should be described solely by name; describe more complex techniques in the Methods section.*
☒	☐	A description of all covariates tested
☒	☐	A description of any assumptions or corrections, such as tests of normality and adjustment for multiple comparisons
☐	☒	A full description of the statistical parameters including central tendency (e.g. means) or other basic estimates (e.g. regression coefficient) AND variation (e.g. standard deviation) or associated estimates of uncertainty (e.g. confidence intervals)
☒	☐	For null hypothesis testing, the test statistic (e.g. *F*, *t*, *r*) with confidence intervals, effect sizes, degrees of freedom and *P* value noted *Give P values as exact values whenever suitable.*
☒	☐	For Bayesian analysis, information on the choice of priors and Markov chain Monte Carlo settings
☒	☐	For hierarchical and complex designs, identification of the appropriate level for tests and full reporting of outcomes
☐	☒	Estimates of effect sizes (e.g. Cohen's *d*, Pearson's *r*), indicating how they were calculated

Our web collection on statistics for biologists contains articles on many of the points above.

Software and code

Policy information about availability of computer code

Data collection	No software was used for data collection.
Data analysis	CRISPR spacer extraction and mapping software can be accessed at https://github.com/ravisheth/trace. For analysis, we used custom code in Python (version 3.6), relying upon the numpy (1.14.0), scipy (1.1.0), pandas (1.0.3), scikit-learn (0.19.1), matplotlib (2.0.2), and seaborn (0.9.0) packages. GraphPad Prism (v7) was used. USEARCH (11.0.667) and RDP classifier (2.12) were used for processing 16S rRNA sequencing data. iTOL (v4) was used for construction of phylogenetic tree.

For manuscripts utilizing custom algorithms or software that are central to the research but not yet described in published literature, software must be made available to editors and reviewers. We strongly encourage code deposition in a community repository (e.g. GitHub). See the Nature Research guidelines for submitting code & software for further information.

Data

Policy information about availability of data

All manuscripts must include a data availability statement. This statement should provide the following information, where applicable:
- Accession codes, unique identifiers, or web links for publicly available datasets
- A list of figures that have associated raw data
- A description of any restrictions on data availability

All data supporting the findings of this study are available within the article and its supplementary information, or are available from the authors upon request. Sequencing data associated with this study is available at NCBI SRA under PRJNA625964.

Field-specific reporting

Please select the one below that is the best fit for your research. If you are not sure, read the appropriate sections before making your selection.

☒ Life sciences ☐ Behavioural & social sciences ☐ Ecological, evolutionary & environmental sciences

For a reference copy of the document with all sections, see nature.com/documents/nr-reporting-summary-flat.pdf

Life sciences study design

All studies must disclose on these points even when the disclosure is negative.

Sample size	Sample sizes were not pre-calculated. In most cases, sample sizes (n) are at least 3 biological replicates, which is standard in our field, and were determined by accounting for batch variability. The number of independent experiments and biological replicates are described in each figure or its legend.
Data exclusions	No data were excluded in this study.
Replication	All experiments were performed at least two times, on different days, to verify reproducibility. All attempts at replication were successful.
Randomization	Randomization was not performed because genetically identical samples were used.
Blinding	Investigators were not blinded during data collection and analysis due to the quantitative and non-subjective nature of the analyses.

Reporting for specific materials, systems and methods

We require information from authors about some types of materials, experimental systems and methods used in many studies. Here, indicate whether each material, system or method listed is relevant to your study. If you are not sure if a list item applies to your research, read the appropriate section before selecting a response.

Materials & experimental systems

n/a	Involved in the study
☒	☐ Antibodies
☒	☐ Eukaryotic cell lines
☒	☐ Palaeontology and archaeology
☒	☐ Animals and other organisms
☒	☐ Human research participants
☒	☐ Clinical data
☒	☐ Dual use research of concern

Methods

n/a	Involved in the study
☒	☐ ChIP-seq
☒	☐ Flow cytometry
☒	☐ MRI-based neuroimaging

Supplementary information

Robust direct digital-to-biological data storage in living cells

Supplementary Information

Robust direct digital-to-biological data storage in living cells

Sung Sun Yim, Ross M. McBee, Alan M. Song, Yiming Huang, Ravi U. Sheth, Harris H. Wang[*]

*correspondence to: hw2429@columbia.edu

This PDF file includes:

Supplementary Figures 1 to 6

Supplementary Tables 1 to 3
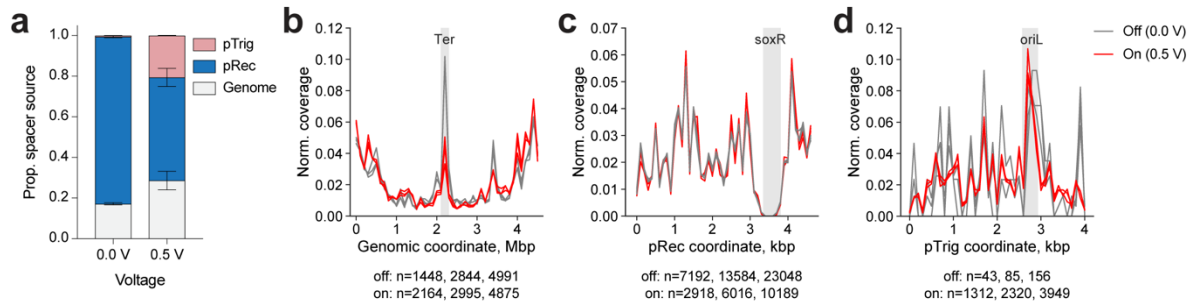
Supplementary Figure 1. Mapping spacers to their source location. (a) Proportion of source of newly incorporated spacers without (off, 0.0 V) and with (on, 0.5 V) electrical signal for 14 hours. **(b)** Genome-derived, **(c)** pRec-derived, and **(d)** pTrig-derived spacers were mapped to their protospacer location. Coverage was summed across 100 kb bins for genome or 100 bp bins for plasmids, and plotted. The three biological replicates without electrical stimulation (off, 0.0 V) are displayed in grey lines, and the three biological replicates with electrical stimulation (on, 0.5 V) are displayed in red lines. Genomic coordinate 0 is indexed as the midpoint of the oriC sequence. Spacers from the *soxR* gene region in pRec is excluded in the analysis as the region is present also in the genome. All measurements are based on three biological replicates. The number of spacers used in the analysis is displayed for each biological replicate.
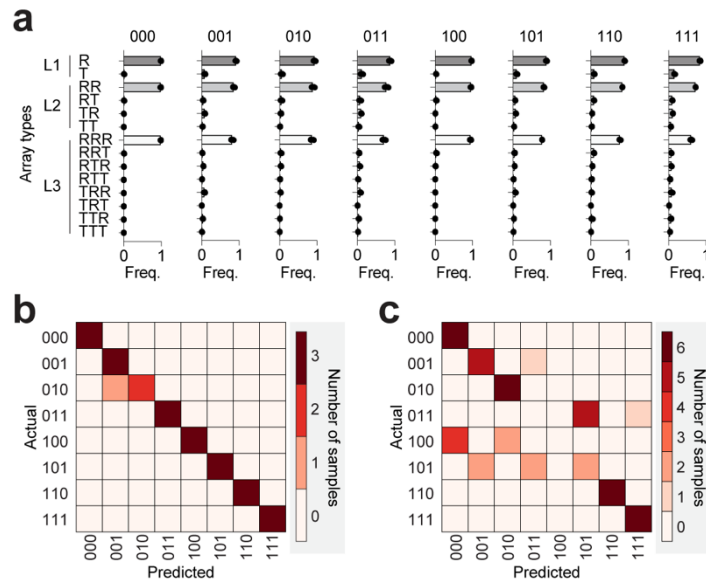
Supplementary Figure 2. Classification using Euclidean distance between observed and reference datasets. For comparison, Euclidean distance between observed (new dataset) and reference array-type frequencies was calculated, and the 3-bit profile with minimum distance to the observed data was selected as the predicted 3-bit profile as previously described in Sheth et al., *Science* **358**, 1457-1461 (2017). **(a)** The reference array-type frequencies (derived from the first three independent experiments described in **Figure 2d**, averaged) used for the classification. The frequencies values are same as in **Figure 2d** but plotted in linear scale. **(b)** Classification of the training datasets (the first three independent datasets that we extracted reference array-type frequencies). For the classification of each sample, average 163,541 of total sequencing reads with 67,620 of expanded arrays (or 23,827 of L2/L3 arrays) with uniquely mapping spacers were used. Bead-based size enrichment was performed to enrich for expanded arrays and deplete unexpanded arrays. **(c)** Classification of the test datasets (6 additional independent datasets). For classification of each sample, an average of 172,788 total sequencing reads with 89,928 reads of expanded arrays (or 38,295 of L2/L3 arrays) that uniquely map spacers were used. Bead-based size enrichment was performed to enrich for expanded arrays and deplete unexpanded arrays.
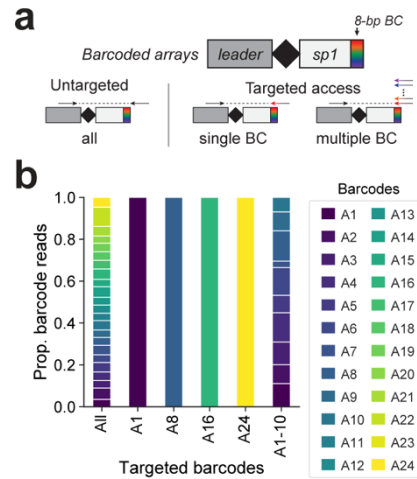
Supplementary Figure 3. Targeted access to specific barcoded cell populations in a mixed pool. (a) Schematic diagram of targeted amplification of barcoded CRISPR arrays in a mixed pool. **(b)** Targeted access to single or multiple barcoded cell populations in a mixed pool of 24 barcoded cell populations. For the targeted access to multiple (A1-10) barcoded cell populations, a single PCR reaction was performed using multiple primers simultaneously. All measurements are based on a single biological replicate.
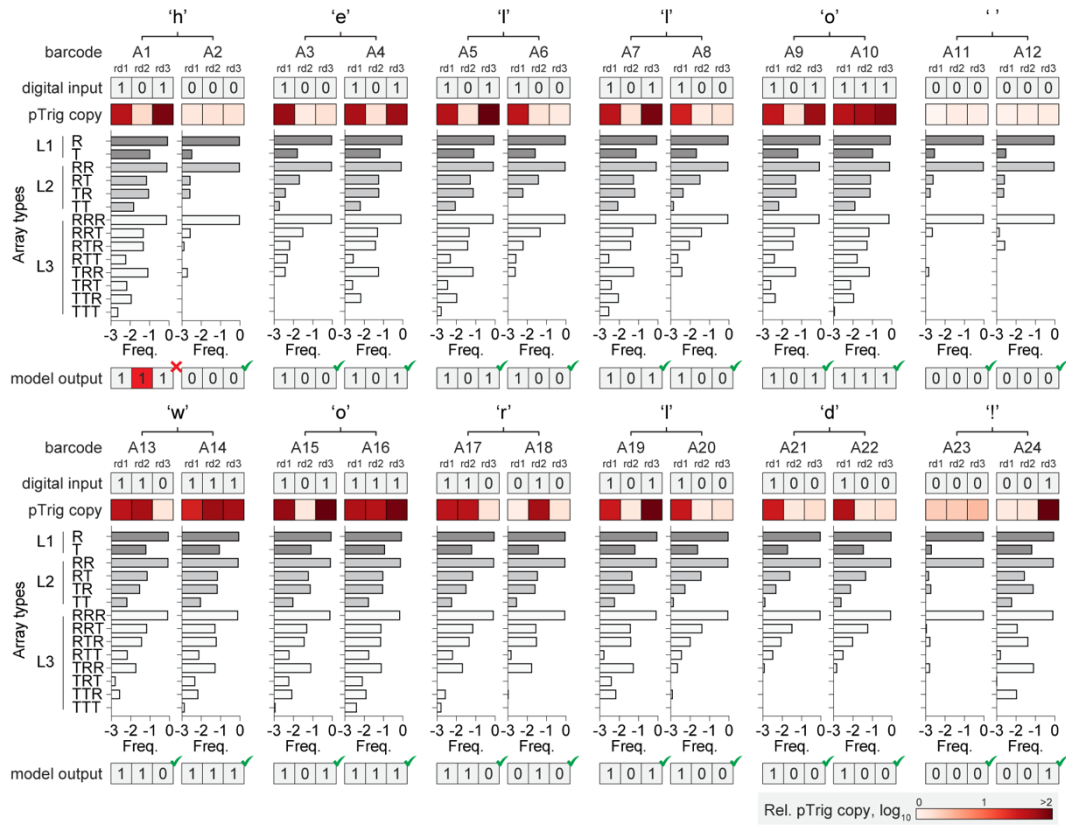
Supplementary Figure 4. 'hello world!' encoded in barcoded *E. coli* populations by DEC 6-bit encoding. DEC 6-bit encoding table is expected to have higher error rates for data reconstruction as described in **Extended Data Fig. 7**. When the same 'hello world!' text message was encoded using DEC 6-bit encoding table, 1 bit out of 72 bits for the text message was misclassified, resulting 'xello world!' returned from the classifier instead of 'hello world!'. For classification of each barcoded cell population, an average of 247,906 total sequencing reads with 147,073 reads of expanded arrays (or 102,475 of L2/L3 arrays) that uniquely map spacers were used. Bead-based size enrichment was performed to enrich for expanded arrays and deplete unexpanded arrays. Frequencies of array-types are in $\log_{10}$ scale. All measurements are based on a single experimental study.
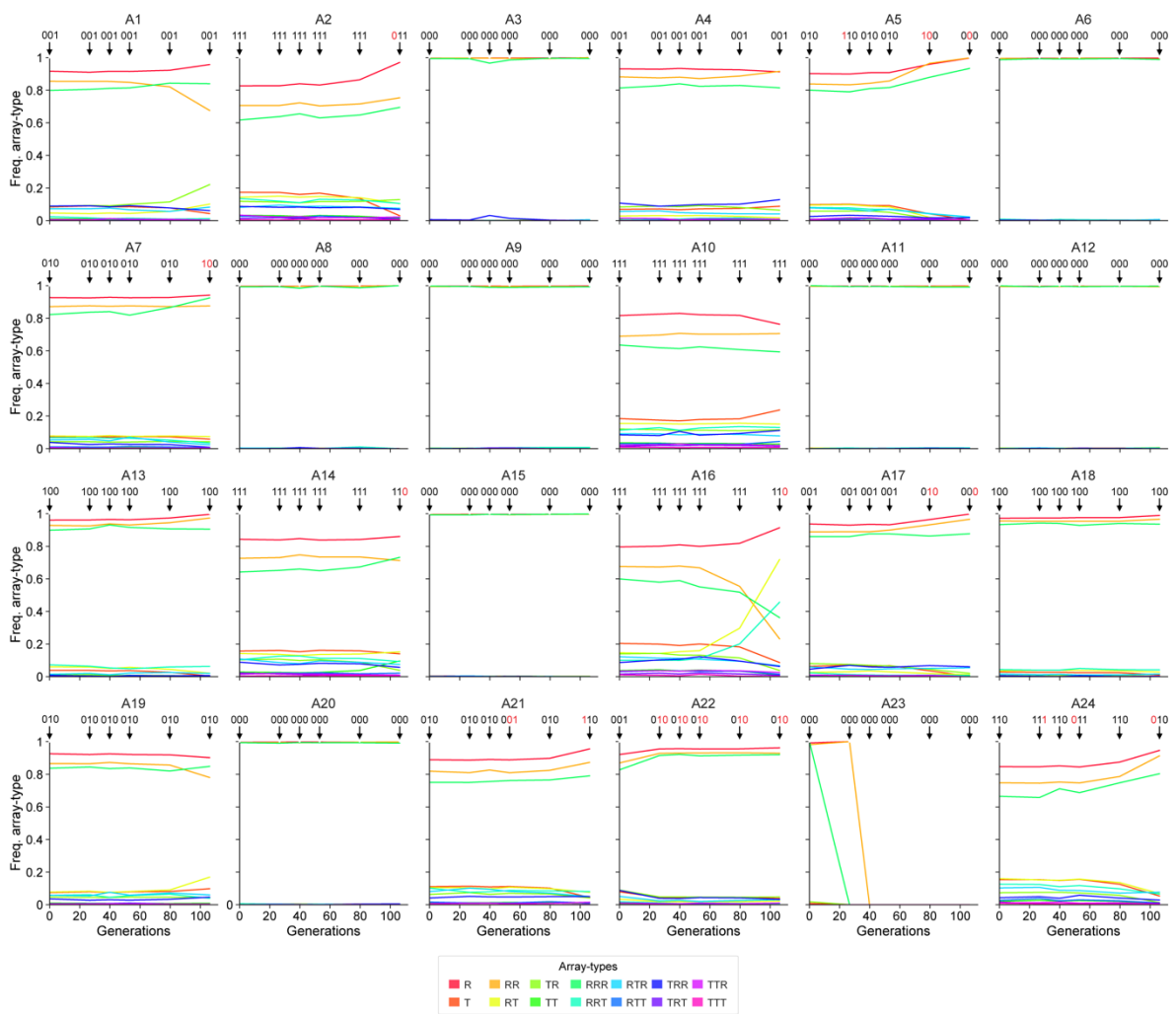
Supplementary Figure 5. Array-type fluctuations over time in replicating cells. The array-type frequencies for each array lengths in each barcoded cell population over the course of the passage experiment in **Extended Data Fig. 10** are plotted. Samples were collected at the time points indicated by arrows (day 0, 4, 6, 8, 12, and 16). For each sampling time point, the measured array-type frequencies were used for data retrieval and the classification results are displayed (black: correct, red: wrong). For classification of each sample, an average of 82,860 total sequencing reads with 40,502 reads of expanded arrays (or 17,139 of L2/L3 arrays) that uniquely map spacers were used. Bead-based size enrichment was performed to enrich for expanded arrays and deplete unexpanded arrays. All measurements are based on three biological replicates.
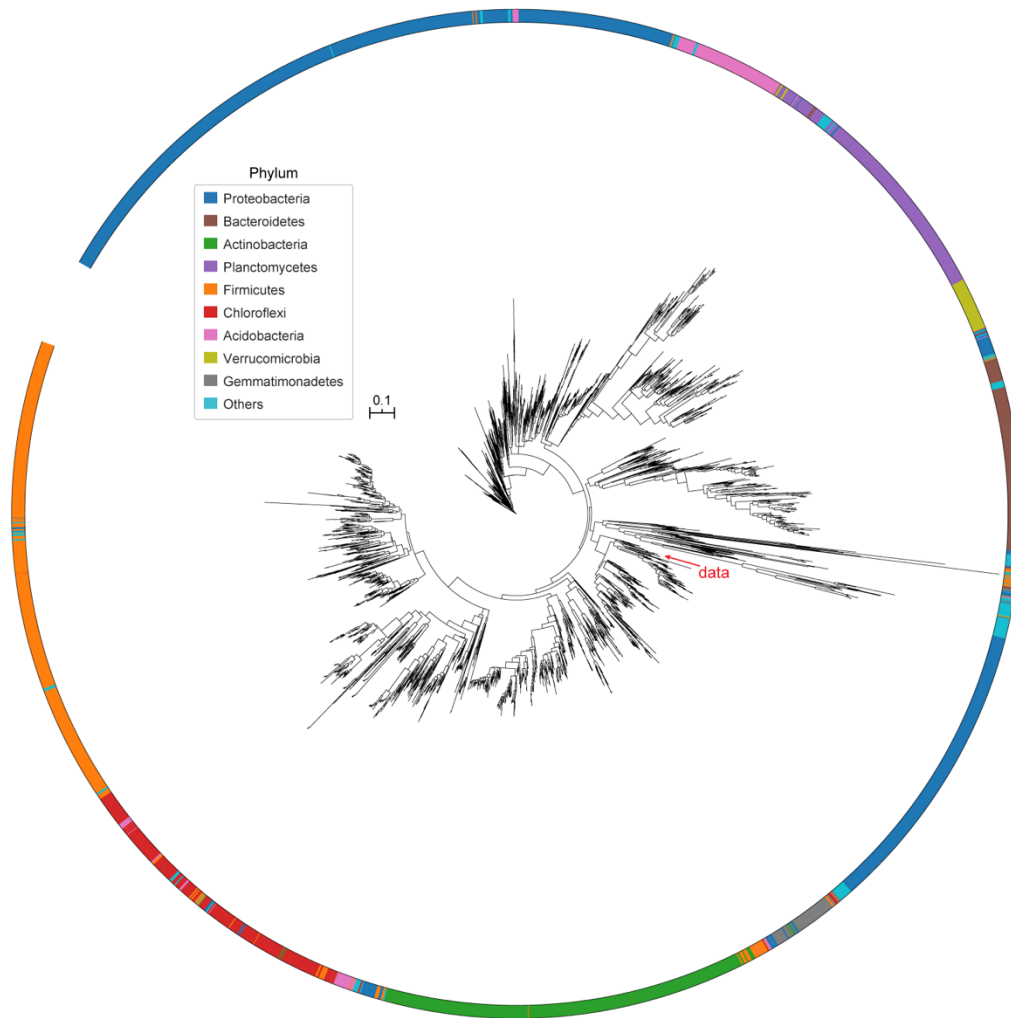
Supplementary Figure 6. Phylogenetic diversity of a mixed microbial community of data-encoded *E. coli* cells and natural soil microbiota. Maximum-likelihood phylogenetic tree of all 4083 OTUs detected in the mixed community based on multiple sequence alignment of V4 region of 16S rRNA sequences using MAFFT (distance scale of 0.1).

Supplementary Table 1. Barcodes for CRISPR arrays

Array#	Array_sequence	BC
A1	TGTTGTTTGTGTGATACTATAAAGTTGGTAGATTGTGACTGGCTTAAAAAATCATTAATTAATAATAGGTTATGTTTAGAGTGTTCCCCG CGCCAGCGGGGATAAACCGAGCACAAATATCATCGCTCAAACCACTTACGGTAAGGCGATCTAATCTAGCGCGACGTC	TAAG GCGA
A2	TGTTGTTTGTGTGATACTATAAAGTTGGTAGATTGTGACTGGCTTAAAAAATCATTAATTAATAATAGGTTATGTTTAGAGTGTTCCCCG CGCCAGCGGGGATAAACCGAGCACAAATATCATCGCTCAAACCACTTACGGCGTACTAGTCTAATCTAGCGCGACGTC	CGTA CTAG
A3	TGTTGTTTGTGTGATACTATAAAGTTGGTAGATTGTGACTGGCTTAAAAAATCATTAATTAATAATAGGTTATGTTTAGAGTGTTCCCCG CGCCAGCGGGGATAAACCGAGCACAAATATCATCGCTCAAACCACTTACGGAGGCAGAATCTAATCTAGCGCGACGTC	AGGC AGAA
A4	TGTTGTTTGTGTGATACTATAAAGTTGGTAGATTGTGACTGGCTTAAAAAATCATTAATTAATAATAGGTTATGTTTAGAGTGTTCCCCG CGCCAGCGGGGATAAACCGAGCACAAATATCATCGCTCAAACCACTTACGGTCCTGAGCTCTAATCTAGCGCGACGTC	TCCT GAGC
A5	TGTTGTTTGTGTGATACTATAAAGTTGGTAGATTGTGACTGGCTTAAAAAATCATTAATTAATAATAGGTTATGTTTAGAGTGTTCCCCG CGCCAGCGGGGATAAACCGAGCACAAATATCATCGCTCAAACCACTTACGGGGACTCCTTCTAATCTAGCGCGACGTC	GGAC TCCT
A6	TGTTGTTTGTGTGATACTATAAAGTTGGTAGATTGTGACTGGCTTAAAAAATCATTAATTAATAATAGGTTATGTTTAGAGTGTTCCCCG CGCCAGCGGGGATAAACCGAGCACAAATATCATCGCTCAAACCACTTACGGTAGGCATGTCTAATCTAGCGCGACGTC	TAGG CATG
A7	TGTTGTTTGTGTGATACTATAAAGTTGGTAGATTGTGACTGGCTTAAAAAATCATTAATTAATAATAGGTTATGTTTAGAGTGTTCCCCG CGCCAGCGGGGATAAACCGAGCACAAATATCATCGCTCAAACCACTTACGGCTCTCTACTCTAATCTAGCGCGACGTC	CTCT CTAC
A8	TGTTGTTTGTGTGATACTATAAAGTTGGTAGATTGTGACTGGCTTAAAAAATCATTAATTAATAATAGGTTATGTTTAGAGTGTTCCCCG CGCCAGCGGGGATAAACCGAGCACAAATATCATCGCTCAAACCACTTACGGCGAGGCTGTCTAATCTAGCGCGACGTC	CGAG GCTG
A9	TGTTGTTTGTGTGATACTATAAAGTTGGTAGATTGTGACTGGCTTAAAAAATCATTAATTAATAATAGGTTATGTTTAGAGTGTTCCCCG CGCCAGCGGGGATAAACCGAGCACAAATATCATCGCTCAAACCACTTACGGAAGAGGCATCTAATCTAGCGCGACGTC	AAGA GGCA
A10	TGTTGTTTGTGTGATACTATAAAGTTGGTAGATTGTGACTGGCTTAAAAAATCATTAATTAATAATAGGTTATGTTTAGAGTGTTCCCCG CGCCAGCGGGGATAAACCGAGCACAAATATCATCGCTCAAACCACTTACGGGTAGAGGATCTAATCTAGCGCGACGTC	GTAG AGGA
A11	TGTTGTTTGTGTGATACTATAAAGTTGGTAGATTGTGACTGGCTTAAAAAATCATTAATTAATAATAGGTTATGTTTAGAGTGTTCCCCG CGCCAGCGGGGATAAACCGAGCACAAATATCATCGCTCAAACCACTTACGGGCTCATGATCTAATCTAGCGCGACGTC	GCTC ATGA
A12	TGTTGTTTGTGTGATACTATAAAGTTGGTAGATTGTGACTGGCTTAAAAAATCATTAATTAATAATAGGTTATGTTTAGAGTGTTCCCCG CGCCAGCGGGGATAAACCGAGCACAAATATCATCGCTCAAACCACTTACGGATCTCAGGTCTAATCTAGCGCGACGTC	ATCT CAGG
A13	TGTTGTTTGTGTGATACTATAAAGTTGGTAGATTGTGACTGGCTTAAAAAATCATTAATTAATAATAGGTTATGTTTAGAGTGTTCCCCG CGCCAGCGGGGATAAACCGAGCACAAATATCATCGCTCAAACCACTTACGGACTCGCTATCTAATCTAGCGCGACGTC	ACTC GCTA
A14	TGTTGTTTGTGTGATACTATAAAGTTGGTAGATTGTGACTGGCTTAAAAAATCATTAATTAATAATAGGTTATGTTTAGAGTGTTCCCCG CGCCAGCGGGGATAAACCGAGCACAAATATCATCGCTCAAACCACTTACGGGGAGCTACTCTAATCTAGCGCGACGTC	GGAG CTAC
A15	TGTTGTTTGTGTGATACTATAAAGTTGGTAGATTGTGACTGGCTTAAAAAATCATTAATTAATAATAGGTTATGTTTAGAGTGTTCCCCG CGCCAGCGGGGATAAACCGAGCACAAATATCATCGCTCAAACCACTTACGGGCGTAGTATCTAATCTAGCGCGACGTC	GCGT AGTA
A16	TGTTGTTTGTGTGATACTATAAAGTTGGTAGATTGTGACTGGCTTAAAAAATCATTAATTAATAATAGGTTATGTTTAGAGTGTTCCCCG CGCCAGCGGGGATAAACCGAGCACAAATATCATCGCTCAAACCACTTACGGCGGAGCCTTCTAATCTAGCGCGACGTC	CGGA GCCT
A17	TGTTGTTTGTGTGATACTATAAAGTTGGTAGATTGTGACTGGCTTAAAAAATCATTAATTAATAATAGGTTATGTTTAGAGTGTTCCCCG CGCCAGCGGGGATAAACCGAGCACAAATATCATCGCTCAAACCACTTACGGTACGCTGCTCTAATCTAGCGCGACGTC	TACG CTGC
A18	TGTTGTTTGTGTGATACTATAAAGTTGGTAGATTGTGACTGGCTTAAAAAATCATTAATTAATAATAGGTTATGTTTAGAGTGTTCCCCG CGCCAGCGGGGATAAACCGAGCACAAATATCATCGCTCAAACCACTTACGGATGCGCAGTCTAATCTAGCGCGACGTC	ATGC GCAG
A19	TGTTGTTTGTGTGATACTATAAAGTTGGTAGATTGTGACTGGCTTAAAAAATCATTAATTAATAATAGGTTATGTTTAGAGTGTTCCCCG CGCCAGCGGGGATAAACCGAGCACAAATATCATCGCTCAAACCACTTACGGTAGCGCTCTCTAATCTAGCGCGACGTC	TAGC GCTC
A20	TGTTGTTTGTGTGATACTATAAAGTTGGTAGATTGTGACTGGCTTAAAAAATCATTAATTAATAATAGGTTATGTTTAGAGTGTTCCCCG CGCCAGCGGGGATAAACCGAGCACAAATATCATCGCTCAAACCACTTACGGACTGAGCGTCTAATCTAGCGCGACGTC	ACTG AGCG
A21	TGTTGTTTGTGTGATACTATAAAGTTGGTAGATTGTGACTGGCTTAAAAAATCATTAATTAATAATAGGTTATGTTTAGAGTGTTCCCCG CGCCAGCGGGGATAAACCGAGCACAAATATCATCGCTCAAACCACTTACGGCCTAAGACTCTAATCTAGCGCGACGTC	CCTA AGAC
A22	TGTTGTTTGTGTGATACTATAAAGTTGGTAGATTGTGACTGGCTTAAAAAATCATTAATTAATAATAGGTTATGTTTAGAGTGTTCCCCG CGCCAGCGGGGATAAACCGAGCACAAATATCATCGCTCAAACCACTTACGGCGATCAGTTCTAATCTAGCGCGACGTC	CGAT CAGT
A23	TGTTGTTTGTGTGATACTATAAAGTTGGTAGATTGTGACTGGCTTAAAAAATCATTAATTAATAATAGGTTATGTTTAGAGTGTTCCCCG CGCCAGCGGGGATAAACCGAGCACAAATATCATCGCTCAAACCACTTACGGTGCAGCTATCTAATCTAGCGCGACGTC	TGCA GCTA
A24	TGTTGTTTGTGTGATACTATAAAGTTGGTAGATTGTGACTGGCTTAAAAAATCATTAATTAATAATAGGTTATGTTTAGAGTGTTCCCCG CGCCAGCGGGGATAAACCGAGCACAAATATCATCGCTCAAACCACTTACGGTCGACGTCTCTAATCTAGCGCGACGTC	TCGA CGTC

Colors: Leader-DR-Spacer1-BC-Pad

Supplementary Table 2. Simple parity check error correction

Actual input: 00000[0] / Error corrected output: 00000[0] (100%)

Possible 1st 3-bit call	Possible 2nd 3-bit call	Prediction probability	# of 1 in the 1st 5 bits	Checksum	Checksum correct?	Can be recovered properly?
000	00[0]	100%	0	0	T	T

Actual input: 00001[1] / Error corrected output: 00001[1] (100%)

Possible 1st 3-bit call	Possible 2nd 3-bit call	Prediction probability	# of 1 in the first 5 bits	Checksum	Checksum correct?	Can be recovered properly?
000	01[1]	83.33%	1	1	T	T
000	00[1]	16.67%	0	0	F	T

Actual input: 00010[1] / Error corrected output: 00010[1] (100%)

Possible 1st 3-bit call	Possible 2nd 3-bit call	Prediction probability	# of 1 in the first 5 bits	Checksum	Checksum correct?	Can be recovered properly?
000	10[1]	83.33%	1	1	T	T
000	11[1]	16.67%	2	0	F	T

Actual input: 00011[0] / Error corrected output: 00011[0] (100%)

Possible 1st 3-bit call	Possible 2nd 3-bit call	Prediction probability	# of 1 in the first 5 bits	Expected checksum	Checksum correct?	Can be recovered properly?
000	11[0]	83.33%	2	0	T	T
000	01[0]	16.67%	1	1	F	T

Actual input: 00100[1] / Error corrected output: 00100[1] (100%)

Possible 1st 3-bit call	Possible 2nd 3-bit call	Prediction probability	# of 1 in the first 5 bits	Expected checksum	Checksum correct?	Can be recovered properly?
001	00[1]	100%	1	1	T	T

Actual input: 00101[0] / Error corrected output: 00101[0] (100%)

Possible 1st 3-bit call	Possible 2nd 3-bit call	Prediction probability	# of 1 in the first 5 bits	Expected checksum	Checksum correct?	Can be recovered properly?
001	01[0]	100%	2	0	T	T

Actual input: 00110[0] / Error corrected output: 00110[0] (100%)

Possible 1st 3-bit call	Possible 2nd 3-bit call	Prediction probability	# of 1 in the first 5 bits	Expected checksum	Checksum correct?	Can be recovered properly?
001	10[0]	100%	2	0	T	T

Actual input: 00111[1] / Error corrected output: 00111[1] (100%)

Possible 1st 3-bit call	Possible 2nd 3-bit call	Prediction probability	# of 1 in the first 5 bits	Expected checksum	Checksum correct?	Can be recovered properly?
001	11[1]	100%	3	1	T	T

Actual input: 01000[1] / Error corrected output: 01000[1] (100%)

Possible 1st 3-bit call	Possible 2nd 3-bit call	Prediction probability	# of 1 in the first 5 bits	Expected checksum	Checksum correct?	Can be recovered properly?
010	00[1]	100%	1	1	T	T

Actual input: 01001[0] / Error corrected output: 01001[0] (100%)

Possible 1st 3-bit call	Possible 2nd 3-bit call	Prediction probability	# of 1 in the first 5 bits	Expected checksum	Checksum correct?	Can be recovered properly?
010	01[0]	100%	2	0	T	T

Actual input: 01010[0] / Error corrected output: 01010[0] (100%)

Possible 1st 3-bit call	Possible 2nd 3-bit call	Prediction probability	# of 1 in the first 5 bits	Expected checksum	Checksum correct?	Can be recovered properly?
010	10[0]	100%	2	0	T	T

Actual input: 01011[1] / Error corrected output: 01011[1] (100%)

Possible 1st 3-bit call	Possible 2nd 3-bit call	Prediction probability	# of 1 in the first 5 bits	Expected checksum	Checksum correct?	Can be recovered properly?
010	11[1]	100%	3	1	T	T

Actual input: 01100[0] / Error corrected output: 01100[0] (100%)

Possible 1st 3-bit call	Possible 2nd 3-bit call	Prediction probability	# of 1 in the first 5 bits	Expected checksum	Checksum correct?	Can be recovered properly?
011	00[0]	83.33%	2	0	T	T
001	00[0]	16.67%	1	1	F	T

Actual input: 01101[1] / Error corrected output: 01101[1] (97.22%), 00100[1] (2.78%)

Possible 1st 3-bit call	Possible 2nd 3-bit call	Prediction probability	# of 1 in the first 5 bits	Expected checksum	Checksum correct?	Can be recovered properly?
011	01[1]	69.44%	3	1	T	T
011	00[1]	13.89%	2	0	F	T
001	01[1]	13.89%	2	0	F	T
001	00[1]	2.78%	1	1	T	F

Actual input: 01110[1] / Error corrected output: 01110[1] (97.22%), 00111[1] (2.78%)

Possible 1st 3-bit call	Possible 2nd 3-bit call	Prediction probability	# of 1 in the first 5 bits	Expected checksum	Checksum correct?	Can be recovered properly?
011	10[1]	69.44%	3	1	T	T
011	11[1]	13.89%	4	0	F	T
001	10[1]	13.89%	2	0	F	T
001	11[1]	2.78%	3	1	T	F

Actual input: 01111[0] / Error corrected output: 01111[0] (97.22%), 00101[0] (2.78%)

Possible 1st 3-bit call	Possible 2nd 3-bit call	Prediction probability	# of 1 in the first 5 bits	Expected checksum	Checksum correct?	Can be recovered properly?
011	11[0]	69.44%	4	0	T	T
011	01[0]	13.89%	3	1	F	T
001	11[0]	13.89%	3	1	F	T
001	01[0]	2.78%	2	0	T	F

Actual input: 10000[1] / Error corrected output: 10000[1] (100%)

Possible 1st 3-bit call	Possible 2nd 3-bit call	Prediction probability	# of 1 in the first 5 bits	Expected checksum	Checksum correct?	Can be recovered properly?
100	00[1]	100%	1	1	T	T

Actual input: 10001[0] / Error corrected output: 10001[0] (100%)

Possible 1st 3-bit call	Possible 2nd 3-bit call	Prediction probability	# of 1 in the first 5 bits	Expected checksum	Checksum correct?	Can be recovered properly?
100	01[0]	100%	2	0	T	T

Actual input: 10010[0] / Error corrected output: 10010[0] (100%)

Possible 1st 3-bit call	Possible 2nd 3-bit call	Prediction probability	# of 1 in the first 5 bits	Expected checksum	Checksum correct?	Can be recovered properly?
100	10[0]	100%	2	0	T	T

Actual input: 10011[1] / Error corrected output: 10011[1] (100%)

Possible 1st 3-bit call	Possible 2nd 3-bit call	Prediction probability	# of 1 in the first 5 bits	Expected checksum	Checksum correct?	Can be recovered properly?
100	11[1]	100%	3	1	T	T

Actual input: 10100[0] / Error corrected output: 10100[0] (100%)

Possible 1st 3-bit call	Possible 2nd 3-bit call	Prediction probability	# of 1 in the first 5 bits	Expected checksum	Checksum correct?	Can be recovered properly?
101	00[0]	83.33%	2	0	T	T
111	00[0]	16.67%	3	1	F	T

Actual input: 10101[1] / Error corrected output: 10101[1] (97.22%), 11100[1] (2.78%)

Possible 1st 3-bit call	Possible 2nd 3-bit call	Prediction probability	# of 1 in the first 5 bits	Expected checksum	Checksum correct?	Can be recovered properly?
101	01[1]	69.44%	3	1	T	T
101	00[1]	13.89%	2	0	F	T
111	01[1]	13.89%	4	0	F	T
111	00[1]	2.78%	3	1	T	F

Actual input: 10110[1] / Error corrected output: 10110[1] (97.22%), 11111[1] (2.78%)

Possible 1st 3-bit call	Possible 2nd 3-bit call	Prediction probability	# of 1 in the first 5 bits	Expected checksum	Checksum correct?	Can be recovered properly?
101	10[1]	69.44%	3	1	T	T
101	11[1]	13.89%	4	0	F	T
111	10[1]	13.89%	4	0	F	T
111	11[1]	2.78%	5	1	T	F

Actual input: 10111[0] / Error corrected output: 10111[0] (97.22%), 11101[0] (2.78%)

Possible 1st 3-bit call	Possible 2nd 3-bit call	Prediction probability	# of 1 in the first 5 bits	Expected checksum	Checksum correct?	Can be recovered properly?
101	11[0]	69.44%	4	0	T	T
101	01[0]	13.89%	3	1	F	T
111	11[0]	13.89%	5	1	F	T
111	01[0]	2.78%	4	0	T	F

Actual input: 11000[0] / Error corrected output: 11000[0] (100%)

Possible 1st 3-bit call	Possible 2nd 3-bit call	Prediction probability	# of 1 in the first 5 bits	Expected checksum	Checksum correct?	Can be recovered properly?
110	00[0]	83.33%	2	0	T	T
010	00[0]	16.67%	1	1	F	T

Actual input: 11001[1] / Error corrected output: 11001[1] (97.22%), 01000[1] (2.78%)

Possible 1st 3-bit call	Possible 2nd 3-bit call	Prediction probability	# of 1 in the first 5 bits	Expected checksum	Checksum correct?	Can be recovered properly?
110	01[1]	69.44%	3	1	T	T
110	00[1]	13.89%	2	0	F	T
010	01[1]	13.89%	2	0	F	T
010	00[1]	2.78%	1	1	T	F

Actual input: 11010[1] / Error corrected output: 11010[1] (97.22%), 01011[1] (2.78%)

Possible 1st 3-bit call	Possible 2nd 3-bit call	Prediction probability	# of 1 in the first 5 bits	Expected checksum	Checksum correct?	Can be recovered properly?
110	10[1]	69.44%	3	1	T	T
110	11[1]	13.89%	4	0	F	T
010	10[1]	13.89%	2	0	F	T
010	11[1]	2.78%	3	1	T	F

Actual input: 11011[0] / Error corrected output: 11011[0] (97.22%), 01001[0] (2.78%)

Possible 1st 3-bit call	Possible 2nd 3-bit call	Prediction probability	# of 1 in the first 5 bits	Expected checksum	Checksum correct?	Can be recovered properly?
110	11[0]	69.44%	4	0	T	T
110	01[0]	13.89%	3	1	F	T
010	11[0]	13.89%	3	1	F	T
010	01[0]	2.78%	2	0	T	F

Actual input: 11100[1] / Error corrected output: 11100[1] (100%)

Possible 1st 3-bit call	Possible 2nd 3-bit call	Prediction probability	# of 1 in the first 5 bits	Expected checksum	Checksum correct?	Can be recovered properly?
111	00[1]	100%	3	1	T	T

Actual input: 11101[0] / Error corrected output: 11101[0] (100%)

Possible 1st 3-bit call	Possible 2nd 3-bit call	Prediction probability	# of 1 in the first 5 bits	Expected checksum	Checksum correct?	Can be recovered properly?
111	01[0]	100%	4	0	T	T

Actual input: 11110[0] / Error corrected output: 11110[0] (100%)

Possible 1st 3-bit call	Possible 2nd 3-bit call	Prediction probability	# of 1 in the first 5 bits	Expected checksum	Checksum correct?	Can be recovered properly?
111	10[0]	100%	4	0	T	T

Actual input: 11111[1] / Error corrected output: 11111[1] (100%)

Possible 1st 3-bit call	Possible 2nd 3-bit call	Prediction probability	# of 1 in the first 5 bits	Expected checksum	Checksum correct?	Can be recovered properly?
111	11[1]	100%	5	1	T	T

Supplementary Table 3. Primers used in this study

Seq_primer	Sequence
CB501	AATGATACGGCGACCACCGAGATCTACACTAGATCGCctggcttaaaaaatcattaattaataataggttatgtttaga
CB502	AATGATACGGCGACCACCGAGATCTACACCTCTCTATctggcttaaaaaatcattaattaataataggttatgtttaga
CB503	AATGATACGGCGACCACCGAGATCTACACTATCCTCTctggcttaaaaaatcattaattaataataggttatgtttaga
CB504	AATGATACGGCGACCACCGAGATCTACACAGAGTAGActggcttaaaaaatcattaattaataataggttatgtttaga
CB505	AATGATACGGCGACCACCGAGATCTACACGTAAGGAGctggcttaaaaaatcattaattaataataggttatgtttaga
CB506	AATGATACGGCGACCACCGAGATCTACACACTGCATActggcttaaaaaatcattaattaataataggttatgtttaga
CB507	AATGATACGGCGACCACCGAGATCTACACAAGGAGTActggcttaaaaaatcattaattaataataggttatgtttaga
CB508	AATGATACGGCGACCACCGAGATCTACACCTAAGCCTctggcttaaaaaatcattaattaataataggttatgtttaga
CB509	AATGATACGGCGACCACCGAGATCTACACCGTCTAATctggcttaaaaaatcattaattaataataggttatgtttaga
CB510	AATGATACGGCGACCACCGAGATCTACACTCTCTCCGctggcttaaaaaatcattaattaataataggttatgtttaga
CB511	AATGATACGGCGACCACCGAGATCTACACTCGACTAGctggcttaaaaaatcattaattaataataggttatgtttaga
CB512	AATGATACGGCGACCACCGAGATCTACACTTCTAGCTctggcttaaaaaatcattaattaataataggttatgtttaga
CB513	AATGATACGGCGACCACCGAGATCTACACCCTAGAGTctggcttaaaaaatcattaattaataataggttatgtttaga
CB514	AATGATACGGCGACCACCGAGATCTACACGCGTAAGActggcttaaaaaatcattaattaataataggttatgtttaga
CB515	AATGATACGGCGACCACCGAGATCTACACCTATTAAGctggcttaaaaaatcattaattaataataggttatgtttaga
CB516	AATGATACGGCGACCACCGAGATCTACACAAGGCTATctggcttaaaaaatcattaattaataataggttatgtttaga
CB701	CAAGCAGAAGACGGCATACGAGATTCGCCTTAggtttgagcgatgatatttgtgct
CB702	CAAGCAGAAGACGGCATACGAGATCTAGTACGggtttgagcgatgatatttgtgct
CB703	CAAGCAGAAGACGGCATACGAGATTTCTGCCTggtttgagcgatgatatttgtgct
CB704	CAAGCAGAAGACGGCATACGAGATGCTCAGGAggtttgagcgatgatatttgtgct
CB705	CAAGCAGAAGACGGCATACGAGATAGGAGTCCggtttgagcgatgatatttgtgct

CB706	CAAGCAGAAGACGGCATACGAGATCATGCCTAggtttgagcgatgatatttgtgct
CB707	CAAGCAGAAGACGGCATACGAGATGTAGAGAGggtttgagcgatgatatttgtgct
CB708	CAAGCAGAAGACGGCATACGAGATCCTCTCTGggtttgagcgatgatatttgtgct
CB709	CAAGCAGAAGACGGCATACGAGATAGCGTAGCggtttgagcgatgatatttgtgct
CB710	CAAGCAGAAGACGGCATACGAGATCAGCCTCGggtttgagcgatgatatttgtgct
CB711	CAAGCAGAAGACGGCATACGAGATTGCCTCTTggtttgagcgatgatatttgtgct
CB712	CAAGCAGAAGACGGCATACGAGATTCCTCTACggtttgagcgatgatatttgtgct
CB713	CAAGCAGAAGACGGCATACGAGATTCATGAGCggtttgagcgatgatatttgtgct
CB714	CAAGCAGAAGACGGCATACGAGATCCTGAGATggtttgagcgatgatatttgtgct
CB715	CAAGCAGAAGACGGCATACGAGATTAGCGAGTggtttgagcgatgatatttgtgct
CB716	CAAGCAGAAGACGGCATACGAGATGTAGCTCCggtttgagcgatgatatttgtgct
CB717	CAAGCAGAAGACGGCATACGAGATTACTACGCggtttgagcgatgatatttgtgct
CB718	CAAGCAGAAGACGGCATACGAGATAGGCTCCGggtttgagcgatgatatttgtgct
CB719	CAAGCAGAAGACGGCATACGAGATGCAGCGTAggtttgagcgatgatatttgtgct
CB720	CAAGCAGAAGACGGCATACGAGATCTGCGCATggtttgagcgatgatatttgtgct
CB721	CAAGCAGAAGACGGCATACGAGATGAGCGCTAggtttgagcgatgatatttgtgct
CB722	CAAGCAGAAGACGGCATACGAGATCGCTCAGTggtttgagcgatgatatttgtgct
CB723	CAAGCAGAAGACGGCATACGAGATGTCTTAGGggtttgagcgatgatatttgtgct
CB724	CAAGCAGAAGACGGCATACGAGATACTGATCGggtttgagcgatgatatttgtgct
CBR1	CTGGCTTAAAAAATCATTAATTAATAATAGGTTATGTTTAGAGTGTTCCCCGCGCCAG
CBI1	CGGGGATAAACCGAGCACAAATATCATCGCTCAAACC

CB5XX: Illumina P5 adaptor sequence-BC (8 bp)-*primer binding site*

CB7XX: Illumina P7 adaptor sequence-BC (8 bp)-*primer binding site*

CBR1: Custom read1 sequencing primer (spiked into well 12)

CBI1: Custom index1 sequencing primer (spiked into well 13)

Barcoded array seq primer	Sequence
BC_Array_CB7	CAAGCAGAAGACGGCATACGAGATGACGTCGCGCTAGATTAGA
BC_Array_CBI	AACCGAGCACAAATATCATCGCTCAAACCACTTACGG

BC_Array_CB7: Illumina P7 adaptor sequence-*primer binding site*

BC_Array_CBI: Custom index1 sequencing primer (spiked into well 13)

Random access seq primer	Sequence
RA701	CAAGCAGAAGACGGCATACGAGATCGCTAGATTAGATCGCCTTA
RA702	CAAGCAGAAGACGGCATACGAGATCGCTAGATTAGACTAGTACG
RA703	CAAGCAGAAGACGGCATACGAGATCGCTAGATTAGATTCTGCCT

RA704	CAAGCAGAAGACGGCATACGAGATCGCTAGATTAGAGCTCAGGA
RA705	CAAGCAGAAGACGGCATACGAGATCGCTAGATTAGAAGGAGTCC
RA706	CAAGCAGAAGACGGCATACGAGATCGCTAGATTAGACATGCCTA
RA707	CAAGCAGAAGACGGCATACGAGATCGCTAGATTAGAGTAGAGAG
RA708	CAAGCAGAAGACGGCATACGAGATCGCTAGATTAGACAGCCTCG
RA709	CAAGCAGAAGACGGCATACGAGATCGCTAGATTAGATGCCTCTT
RA710	CAAGCAGAAGACGGCATACGAGATCGCTAGATTAGATCCTCTAC
RA711	CAAGCAGAAGACGGCATACGAGATCGCTAGATTAGATCATGAGC
RA712	CAAGCAGAAGACGGCATACGAGATCGCTAGATTAGACCTGAGAT
RA713	CAAGCAGAAGACGGCATACGAGATCGCTAGATTAGATAGCGAGT
RA714	CAAGCAGAAGACGGCATACGAGATCGCTAGATTAGAGTAGCTCC
RA715	CAAGCAGAAGACGGCATACGAGATCGCTAGATTAGATACTACGC
RA716	CAAGCAGAAGACGGCATACGAGATCGCTAGATTAGAAGGCTCCG
RA717	CAAGCAGAAGACGGCATACGAGATCGCTAGATTAGAGCAGCGTA
RA718	CAAGCAGAAGACGGCATACGAGATCGCTAGATTAGACTGCGCAT
RA719	CAAGCAGAAGACGGCATACGAGATCGCTAGATTAGAGAGCGCTA
RA720	CAAGCAGAAGACGGCATACGAGATCGCTAGATTAGACGCTCAGT
RA721	CAAGCAGAAGACGGCATACGAGATCGCTAGATTAGAGTCTTAGG
RA722	CAAGCAGAAGACGGCATACGAGATCGCTAGATTAGAACTGATCG
RA723	CAAGCAGAAGACGGCATACGAGATCGCTAGATTAGATAGCTGCA
RA724	CAAGCAGAAGACGGCATACGAGATCGCTAGATTAGAGACGTCGA

qPCR_primer	Sequence
genome-F	GCGAGCGATCCAGAAGATCT
genome-R	GGGTAAAGGATGCCACAGACA
pTrig-F	CGCTCTATGATCCAGTCGATTT
pTrig-R	TCCGTATGCCATGCGTTTAT